

A Tutorial on the Tracking, Telemetry, and Command (TT&C) for Space Missions

Original

A Tutorial on the Tracking, Telemetry, and Command (TT&C) for Space Missions / Modenini, Andrea; Ripani, Barbara. - In: IEEE COMMUNICATIONS SURVEYS AND TUTORIALS. - ISSN 1553-877X. - ELETTRONICO. - 25:3(2023), pp. 1510-1542. [10.1109/COMST.2023.3287431]

Availability:

This version is available at: 11583/2979445 since: 2023-06-20T11:12:30Z

Publisher:

IEEE

Published

DOI:10.1109/COMST.2023.3287431

Terms of use:

This article is made available under terms and conditions as specified in the corresponding bibliographic description in the repository

Publisher copyright

IEEE postprint/Author's Accepted Manuscript

©2023 IEEE. Personal use of this material is permitted. Permission from IEEE must be obtained for all other uses, in any current or future media, including reprinting/republishing this material for advertising or promotional purposes, creating new collecting works, for resale or lists, or reuse of any copyrighted component of this work in other works.

(Article begins on next page)



Exploring HTL pathways in carbohydrate–protein mixture: a study on glucose–glycine interaction

Edoardo Tito¹ · Giuseppe Pipitone¹ · Alessandro H. A. Monteverde Videla¹ · Samir Bensaid¹ · Raffaele Pirone¹

Received: 31 October 2022 / Revised: 31 January 2023 / Accepted: 15 February 2023
© The Author(s) 2023

Abstract

The hydrothermal liquefaction (HTL) of biomass is a strategic process to convert wet and waste feedstocks into liquid biofuel. In this work, we investigated the hydrothermal liquefaction of glucose and glycine, alone and together, to mimic the composition of low-lipid content biomass. Experimental tests were performed in a batch setup in the temperature range of 200–350 °C. As the feeding composition and temperature changed, the distribution among the different phases (gas, solid, biocrude, and aqueous phase) and their compositions were evaluated through different analytical techniques (GC–MS, μ -GC, HPLC). Glucose–glycine showed strongly different interactions with reaction temperature: increased biocrude production at high temperature and increased solid production at low temperature, following a proportionally inverse trend. Biocrude, as well as all the other phases, was observed to be completely different according to the feedstock used. To study how their formation and mutual interactions were affected by the composition of the starting feedstock, consecutive reactions of the generated phases were innovatively carried out. The solid phase generated from glucose–glycine interaction at low temperatures was experimentally observed to be mostly converted into biocrude at high temperatures. Furthermore, no interaction phenomena between the different phases were observed with glucose–glycine, while with glucose alone the co-presence of the molecules in the different phases seemed to be the cause for the lowest biocrude yield at high temperatures. The results obtained in this work can provide new insights into the understanding of hydrothermal liquefaction of low-lipid biomass, pointing out synergetic phenomena among both the biomolecules and the resulting phases.

Keywords Biofuel · Hydrothermal liquefaction · Glucose · Glycine · Interaction mechanisms · Melanoidin

1 Introduction

The production of advanced biofuels from waste biomass has gained much attention as a possible solution to the pressing issues of fossil fuel depletion and global warming. Among different technologies, hydrothermal liquefaction (HTL) has shown interesting performance for energy exploitation of organic waste. HTL is a thermochemical reaction performed in an aqueous environment at subcritical temperature (250–374 °C), pressure high enough to avoid vaporization of the feed (4–25 MPa), and solid/water ratio up to 20 wt% [1, 2]. The target product of HTL is an oily phase (biocrude) that, after upgrading, can be used as a substitute for fossil fuels. Three other sub-products are obtained: a solid phase,

a gas phase rich in CO₂, and an aqueous phase in which residual polar organics are mostly dissolved.

HTL reactivity is strictly linked to the strong changes in water properties that take place near critical conditions, where its dielectric constant decreases while its ionic product increases [3]. The former allows better solubilization of the starting biomass and organic matter generated during the decomposition, by behaving as an apolar solvent; the latter increases H⁺ and OH[−] concentration favoring acid- and base-catalyzed reactions [4]. Furthermore, being performed in an aqueous phase, HTL is particularly advantageous for the valorization of wet waste. In fact, alternative and more established thermochemical technologies (combustion, pyrolysis, and gasification) would require a significant amount of vaporization heat that would negatively affect the overall energy efficiency of the process [5].

Lipids, proteins, and carbohydrates are the main biomolecules that make up the starting biomass. The relative concentration of these macrofamilies was shown to strongly

✉ Giuseppe Pipitone
giuseppe.pipitone@polito.it

¹ Department of Applied Science and Technology, Politecnico Di Torino, Corso Duca Degli Abruzzi 24, 10129 Turin, Italy

influence the yields of HTL products [6]. In particular, an experimental campaign with model compounds conducted by Biller and Ross [7] showed that biocrude increased following the composition trend: lipids > proteins > carbohydrates. One example is lipid-rich algae, which are specifically grown for their good energy efficiency and toward which much attention was directed in the early days of HTL. On the other hand, waste biomass like municipal waste, sewage sludge, and food waste often has a lower lipid content than proteins and carbohydrates. Interestingly, these two families showed a high synergy towards biocrude generation. Although it is known that their strong interaction is traced back to the Maillard reaction [8], it is not yet well known which reaction pathways characterize the interaction between them under HTL conditions. That is, despite the chemistry of the Maillard reaction and its products (i.e., melanoidins) has been investigated over the years, it is not entirely known how they influence the formation of the different HTL phases, their yield, and their composition.

In the last years, great attention has been devoted to understanding the chemical mechanisms of HTL, and three major phases were identified: depolymerization, decomposition, and recombination [6]. Organic macromolecules are firstly depolymerized into their constituents, then further decomposed into small compounds, which are distributed among the different phases, and eventually can recombine through radical reactions into long molecules [6]. As reported above, one key point in this framework is the study of multicomponent systems. This approach is pivotal to better mimic the chemistry of biomass, which, being constituted by different kinds of macromolecules (i.e., polysaccharides, proteins, lipids, etc.), has different reaction pathways than those starting from a single model compound. Despite the importance of this topic, the investigation of these phenomena is still limited [9].

To our knowledge, Minowa et al. [10] studied the carbohydrate–protein interaction combining glucose and glycine for the first time in the 150–350 °C range in a batch reactor; they pointed out that their interaction is manifested through the Maillard reaction (i.e., the chemical reaction between the

amino group of proteins and the carbonyl group of carbohydrates) and the formation of melanoidins as key intermediates. However, the authors did not report any results with pure glucose or glycine in water, so any reasoning on the synergy between the molecules was hindered. Peterson et al. [8] designed a continuous plug-flow reactor to examine the same reaction. The authors found out the influence of the reactor system on the reaction kinetics and the significance of the Maillard reaction in hydrothermal biomass processing; nevertheless, they focused only on glucose and glycine conversion, without evaluating any biocrude (likely due to the low reaction temperature—250 °C) or product yield. Teri et al. [11] tested two model polysaccharides (cornstarch and cellulose) and proteins (albumin and soy protein) observing that the mixture produced higher biocrude yields than the test with model compounds alone, and it was attributed to the Maillard reaction promoting the formation of water-insoluble compounds. Fan et al. [12] studied the interaction between lactose and maltose (two disaccharides) with lysine (a long amino acid with a side chain $(\text{CH}_2)_4\text{NH}_2$) within the temperature range (250–350 °C). They investigated all the phases and concluded that the carbohydrate–protein interaction was attributable to the Maillard reaction producing nitrogen-containing aromatics. However, little was experimentally observed regarding interchange phenomena between the phases. Other examples of works investigating the carbohydrate–protein interactions under HTL conditions can be found in Table 1.

The cited works reported valuable results and shed light on many aspects of the interaction between these two fundamental classes of molecules. However, most of them focus only on the biocrude yield, while the distribution of the remaining phases is often left undiscussed. Furthermore, it remains unclear if the different phases produced during HTL can interact and convert among each other, and how the reaction conditions affect this phenomenon.

To fill this gap, the present work focuses on understanding the reaction mechanisms during HTL of glucose and glycine, as monomers of carbohydrates and proteins, respectively. The study was mainly centered on highlighting the

Table 1 Some studies available in literature on the carbohydrate–protein interaction during HTL

Feedstock	Temperature	Phases investigated	Reference
Glucose–glycine	150–350 °C	Biocrude, aqueous phase, solid and gas yield	[10]
Lactose/maltose–lysine	250–350 °C	Biocrude, aqueous phase, solid and gas yield	[12]
Glucose–glycine	250 °C	Glucose/glycine conversion	[8]
Cellulose–albumin	300–350 °C	Biocrude yield	[11]
Glucose–soy protein	280 °C	Biocrude yield and solid residue	[13]
Glucose–glutamic acid	300 °C	Biocrude, aqueous phase, solid and gas yield	[14]
Cellulose–soy protein	350 °C	Biocrude yield	[15]
Glucose–soy protein	300 °C	Biocrude yield	[16]
Glucose–glycine	200–350 °C	Biocrude, aqueous phase, solid and gas yield	This work

differences, both quantitative and qualitative, registered between all the phases with glucose and glycine alone and in a mixture. In fact, by only focusing on all the generated products it is possible to really deepen the underlying mechanisms.

Glucose and glycine were chosen since they are the most common monosaccharide and the simplest amino acid. The use of monomers was justified by the fact that depolymerization is the first step in HTL, and the use of monomers would facilitate the identification of the different products generated. Tests were performed with single monomers and binary solutions to study the synergistic and antagonistic phenomena in the generated phases. In this way, it was possible to highlight how the co-presence of the two molecules affects the production and distribution between the different phases and their composition. Temperature is well known to be one of the most important parameters in HTL; for this reason, the previous considerations were performed in a wide range of temperatures (200–350 °C) in order to observe whether and how they were affected.

The novelty of this work also lies in the approach followed to detect the interactions among the different phases. In the literature, the multiphase environment of HTL is often modeled and studied according to a lump model based on the different phases produced (solid, gas, biocrude, and aqueous phase) [17–19]. A typical reaction scheme is shown in Fig. 1. According to this approach, each phase could be related to the others by exchange reactions. Although some hypotheses have been formulated in the literature for the interaction between carbohydrates and proteins based on such lump-based models, no direct observation of the interchange between the phases has been observed to the authors' knowledge.

In this work, we aim to enlighten such interactions in a deeper and more direct way. To do so, consecutive tests were planned in order to experimentally confirm the interchange between the phases during HTL. That is, once separated during the first run at low temperature, the biocrude, solid, and

aqueous phases were subjected again to HTL at high temperature in separate tests to see in which phases they were transformed, discriminating their preferential conversion pathways. In this way, it was possible to directly observe how and to what extent the production of each phase was linked to the others as the feedstock composition (glucose or glucose–glycine) changed. This technique thus allows experimental demonstration of the relationships between all the different phases produced during HTL (solids, biocrude, gases, and aqueous solubles) and strengthens the hypothesis that the glucose–glycine interaction develops through different relationships among the phases with respect to glucose and glycine reacting alone.

2 Materials and methods

2.1 HTL tests and product separation

D-(+)-glucose ($\geq 99.5\%$ GC) and glycine (ReagentPlus®) from Sigma-Aldrich were used as reactants. HTL tests were conducted in a batch reactor (Parr 4575A, 500 mL). In a typical experiment, the reactor was loaded with 200 g of a solution of glucose (GLU) or glycine (GLY) with a concentration of 5 wt% (with one reagent alone) or 10 wt% (mixture of reagents with 5 wt% each, namely GLU-GLY). The reactor was purged with three cycles at 7 bar using He, and then was pressurized to 3 bar at ambient temperature. The reaction time was kept fixed at 1 h starting from the time the set point temperature was reached. After cooling, the final pressure value was recorded as a quantification check; the gas was sampled and then the reactor was opened. The liquid contained in the reactor was vacuum-filtered to separate the suspended solid. The permeate was extracted with diethyl ether in three steps (1:1 overall mass ratio); the raffinate was defined as aqueous phase (AP), while the extract phase was dehydrated and evaporated through a rotavapor (B-AP). The reactor, as well as the solid removed from the liquid, was cleaned by washing with ethyl acetate. The ethyl acetate solution was vacuum-filtered. The solid removed by the filter was dried overnight at 105 °C and the resulting product constituted the final solid (S). The ethyl acetate contained in the permeate was dehydrated and evaporated through a rotavapor. The resulting product was defined as B-S and the sum between B-S and B-AP represented the biocrude; for simplicity, biocrude mass yields will be reported as the sum of B-S and B-AP. The choice of using two different solvents for the recovery of B-S and B-AP was due to technical limitations. That is, traces of ethyl acetate in the AP would have led to overlapping with other peaks during HPLC. Moreover, traces of diethyl ether could be easily removed before the consecutive reactions from the AP by leaving it under a chemical hood overnight; thus, no ethyl ether remained and

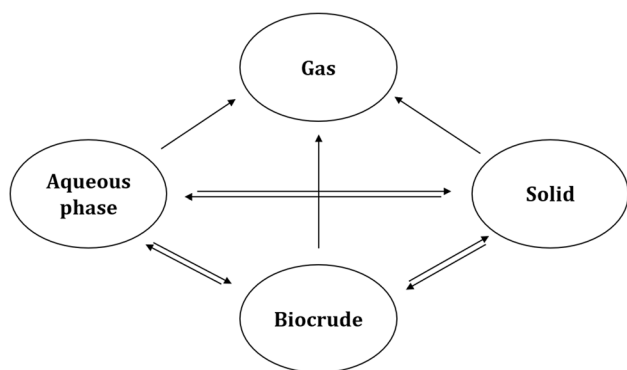


Fig. 1 Possible interchange reactions between phases during HTL

the amount of other compounds did not decrease. On the other hand, using diethyl ether for cleaning the reactor would have been hindered by its low boiling temperature and the long time required for cleaning. An overview of the followed protocol is depicted in Fig. 2.

The mass yield of every phase was evaluated according to Eq. 1, except for the AP yield which was defined as a complement to 100%. An averaged yield (theoretical) was also defined to assess the synergistic/antagonistic behavior of the glucose–glycine interaction (Eq. 2). This value takes into account the experimental yields derived from the tests in which glucose and glycine were alone in the mixture. If a difference between the averaged yields and the experimental yields is present, an interaction between the constituents can be expected. Equations 3 and 4 take account for this difference in absolute and relative form, respectively.

To better understand the correlation between the phases, a campaign of consecutive tests was also performed. The different phases (AP, B-AP, B-S, S) produced at 250 °C for 1 h with GLU, as well with GLU-GLY, were individually re-loaded in the reactor and heated up to 350 °C for 1 h and starting 3 bar of He. Before the reaction, the solid and biocrude, which are insoluble in water, were loaded in the reactor by pouring them with fresh distilled water to obtain a total 200 g solution. On the other hand, the AP was left to mix overnight under the chemical hood to ensure the removal of the residual diethyl ether and then was loaded without dilution.

$$Yield_{phase\ i} (\%) = 100 \cdot \frac{mass_{db, phase\ i}}{mass_{db, reagents}} \quad (1)$$

$$Averaged\ value\ (\%) = \frac{yield_{GLU} + yield_{GLY}}{2} \quad (2)$$

$$Absolute\ difference\ (\%) = yield_{experimental} - yield_{averaged} \quad (3)$$

$$Relative\ difference\ (\%) = \frac{yield_{experimental} - yield_{averaged}}{yield_{experimental}} \quad (4)$$

2.2 Product characterization

The gas phase was analyzed by a Micro-GC (SRA) equipped with Molsieve 5A and PoraPLOT U columns, and a TCD detector. The quantification of the gas phase was based on the final concentration of He (used as an internal standard), according to the ideal gas law.

Organic acids, alcohols, aldehydes, ketones, and sugars dissolved in the aqueous phase were analyzed through HPLC. HPLC analysis (Shimadzu) was performed with a Rezex ROA-Organic acid H+ (8%) column (300 mm · 7.8 mm). The mobile phase was 5 mM H₂SO₄ in water. The flow rate was fixed at 0.7 mL/min and the temperature of the column at 50 °C. The products were determined using

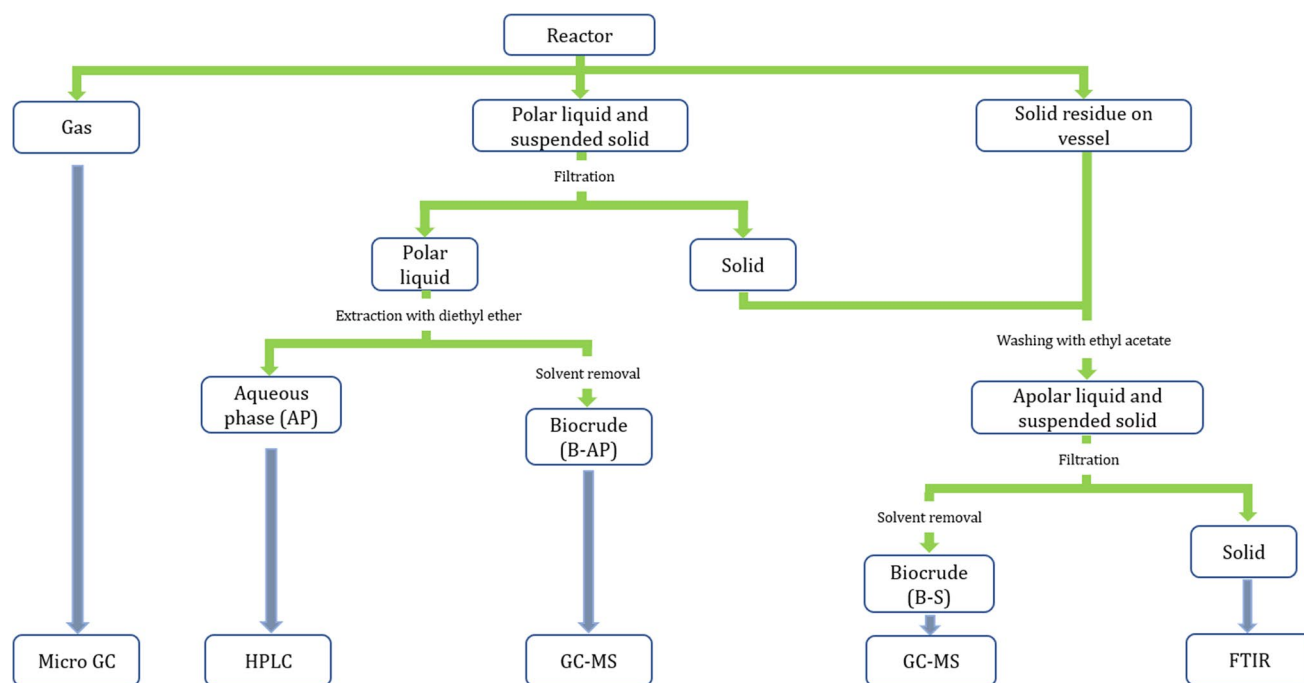


Fig. 2 Work-up (green lines) and analysis (blue lines) after HTL reaction. (The reader is referred to the web version of this paper for the color representation of this figure)

a refractive index detector (RID) and quantified by external calibration using purchased standards.

The oil phases (namely, B-S and B-AP) were characterized using gas chromatography (Agilent Model 7890A) coupled to a mass spectrometer (Agilent Model 5975C). A DB-5 ms column (30 m · 250 μ m · 0.25 μ m) and He as a carrier was used. The injection volume was 0.5 μ L, and the injection port temperature was 290 °C with pulsed splitless mode. The temperature program used for the analysis consisted of a 2-min soak at 40 °C, followed by ramps at 15 °C/min up to 180 °C and a 10-min soak; 3 °C/min up to 230 °C and a 5-min soak; and finally, 15 °C/min up to 300 °C and a 2-min soak. After analysis, the identified compounds were subdivided according to their functionality. If the molecule contained more than one function, a primary and secondary functional group were defined, with a priority order defined as follows: N-containing aromatics > phenol derivatives > benzene derivatives > furan derivatives > amines > cyclic oxygenates > cyclic ketones > esters > aldehydes > ketones > alcohols > ethers. The areas of all compounds belonging to a given group were summed and were presented as a percentage of the sum of the areas of all identified compounds. The sum of the areas of all primary groups gave 100%, while the sum of primary and secondary functional groups gave 100% or more. As an example, given the above-presented priority order, the molecule 2-hydroxy-benzaldehyde would fall within phenols as a core group and aldehydes as a secondary functional group. Compared to the simple identification of the main reactive group, normally found in the literature, the presence of a classification that is also based on the secondary

functional groups allows for a more correct representation of the molecular structures present in the oil phases.

Solid and biocrude properties were also evaluated through thermogravimetric analysis (TGA) and attenuated total reflectance–Fourier transform infrared spectroscopy (ATR-FTIR). TGA was carried out with a Mettler Toledo TGA/SDTA851 thermal gravimetric analyzer, from 25 to 800 °C at a 10 °C/min heating rate and under nitrogen flow (50 mL/min). FTIR spectra were collected with a Bruker Tensor 27 FTIR spectrometer (Bruker Optics, Billerica, Ma), equipped with an attenuated total reflection ATR accessory, between 400 and 400 cm^{-1} wavenumbers and 1 cm^{-1} resolution. The analysis was carried out at room temperature, tightly pressing the sample on the crystal surface.

3 Results and discussion

3.1 Glucose

In Fig. 3A, the product distribution in terms of mass yields for glucose (GLU) is reported at different temperatures.

The gas yield showed an increasing trend with temperature, ending up being almost constant above 300 °C (10 wt%). This trend is in accordance with tests performed by Minowa et al. [20]. As can be seen from Fig. 3B, the gas phase is mainly constituted by CO_2 , with the increasing reaction temperature favoring the formation of H_2 and CO . However, despite the lower CO_2 concentration at high temperatures, its partial pressure increased up to 300 °C and

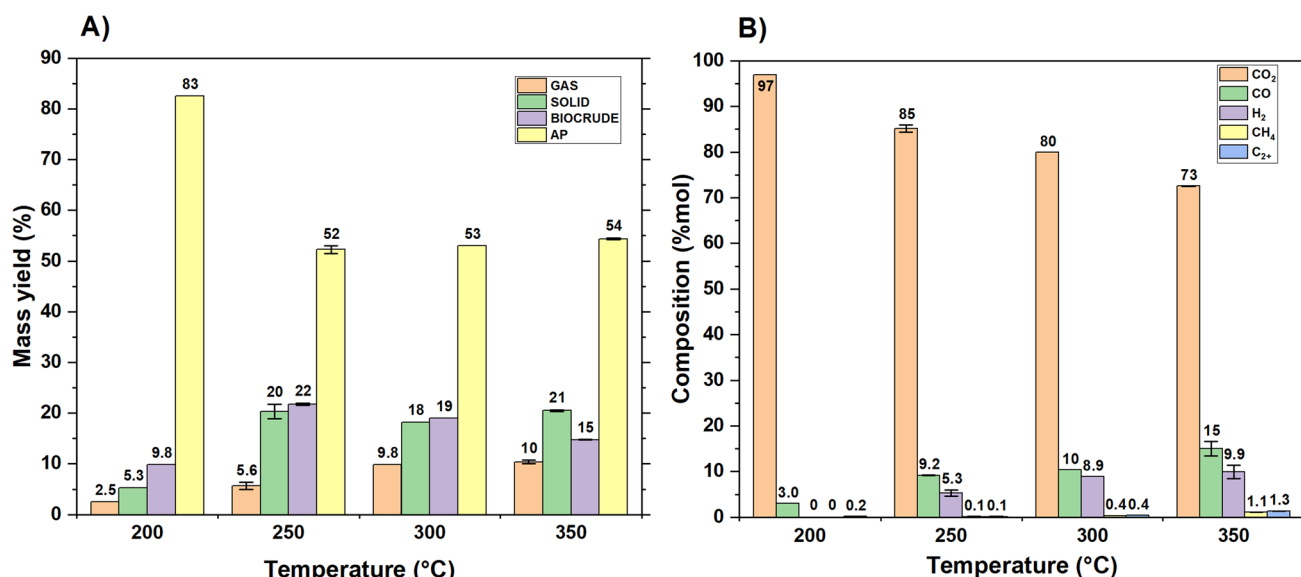


Fig. 3 **A** Mass yields with GLU at different temperatures. **B** Gas compositions (vol. %) for GLU at different temperatures. The term C_{2+} is identified as ethane, ethylene, and propane. Reaction conditions: 5 wt%

glucose, 60 min, 200 g feed. (The reader is referred to the web version of this paper for the color representation of this figure)

then remained constant; all the other compounds showed a stronger increase with temperature.

The differences in gas composition are attributed to the decomposition mechanisms occurring in the liquid and solid phases. Approaching the water critical conditions ($T=374\text{ }^{\circ}\text{C}$), radical-free reactions in the aqueous medium are favored over the ionic ones, enhancing the gas production through the degradation of solid and liquid products [21]. In this way, the slight increase in small alkanes (C1–C3) observed at $350\text{ }^{\circ}\text{C}$ could be explained by the presence of cracking reactions of oil and solid [1]. However, at lower temperatures, radical-free reactions are limited and the raise in CO and H_2 must be traced back to differences in the ratios of decarboxylation, dehydrogenation, and decarbonylation reactions that molecules in the other phases may undergo. In particular, the aqueous phase is usually of more interest in this regard because of molecules such as formic acid and acetic acid that are prone to H_2 , CH_4 , and CO formation [22].

The compounds identified in the aqueous phase are given for every temperature in Figure S1, expressed as carbon yield. At $200\text{ }^{\circ}\text{C}$, unconverted glucose is still detected, accounting for 28% of the feedstock. A high amount of 5-HMF is observed and it derives from glucose through an isomerization/dehydration pathway, which has fructose as a reaction intermediate [20, 23]. The latter was observed in preliminary tests at $150\text{ }^{\circ}\text{C}$, along with 92 percent unconverted glucose and 5-HMF (not shown). Above $200\text{ }^{\circ}\text{C}$, 5-HMF was barely detected in the aqueous phase, while levulinic acid (LA) was identified as the molecule with the highest carbon yield. However, as well as for 5-HMF, LA was also observed in the oil phase as will be shown later on. Traces of 5-HMF and LA observed in the aqueous phase were hence due to an intermediate partition factor of these two molecules into the polar solvents used [24, 25]. LA is the dehydration product from 5-HMF and is produced in equimolar amounts together with formic acid (FA) [26]. However, their molar ratio (FA/LA) is not constant and equal to unity, but instead decreases from 3.0 to 0.03 as the temperature increases from 200 to $350\text{ }^{\circ}\text{C}$. This trend could be due to the conversion of FA to H_2 at high temperatures, given its instability and hydrogen-donor nature.

Looking at the solid phase (Fig. 3A), the mass yield showed an increase with increasing temperature up to $250\text{ }^{\circ}\text{C}$, then reaching a plateau for higher temperature. The HTL-derived solid is generally considered the final product due to the recombination and repolymerization of the reactive fragments generated during the decomposition of biomass polymers [6]. In fact, as the reaction proceeds, hydrogen is less available for capping free radicals, leading to their aggregation and eventually the formation of high molecular weight molecules (char). Approaching supercritical conditions, radical reactions are favored compared to the ionic ones [3]. It should hence be expected an increase in the solid

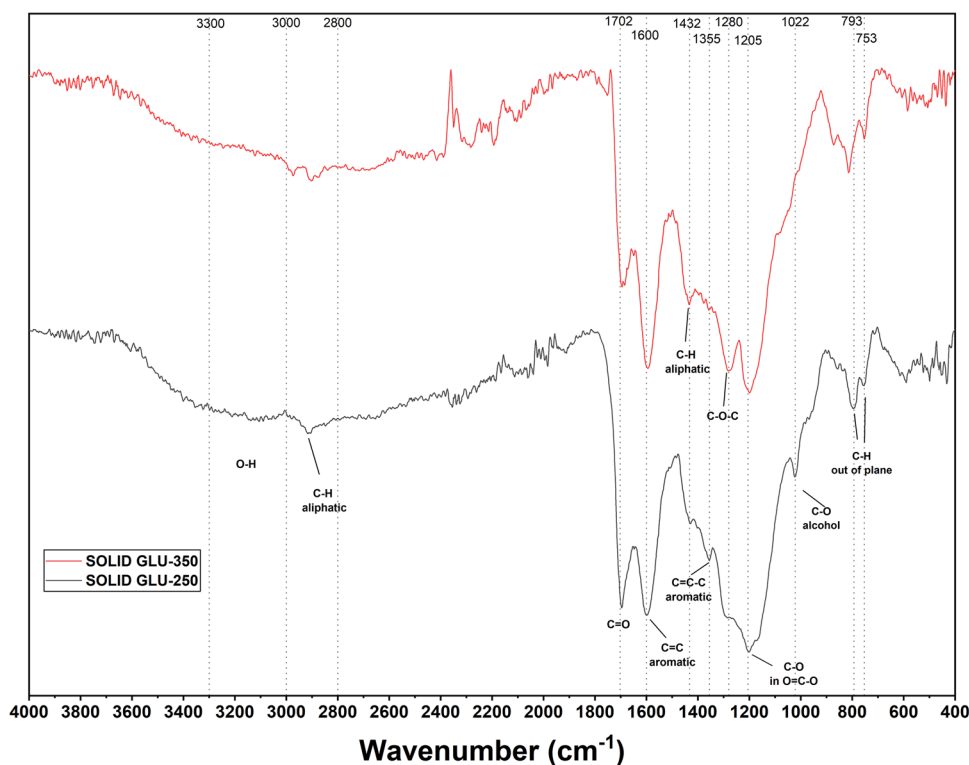
yield with an increase in reaction temperature, as observed by Minowa et al. [20]. However, it was not observed in this work. In this case, the formation of the solid state is probably the result of the formation of intermediate compounds named humins. These are formed through condensation reactions of 5-HMF with glucose and/or a hydrated 5-HMF molecule [27]. The solid observed is hence not assimilable to a carbonaceous structure rich in carbon as char, but rather to a polymeric structure, water-insoluble, still having a fair degree of oxygenation and a certain reactivity. The humin-like structure is confirmed by Fig. 4, reporting the FTIR spectra for the solids obtained at $250\text{ }^{\circ}\text{C}$ and $350\text{ }^{\circ}\text{C}$. The main peaks are attributable to carbonyl groups (1702 cm^{-1} and 1205 cm^{-1}), ether groups (1280 cm^{-1}), and aromatic structures ($\text{C}=\text{C}$ at 1600 cm^{-1} , $\text{C}=\text{C}-\text{C}$ at 1355 cm^{-1} , phenolic $\text{C}-\text{O}$ at 1205 cm^{-1} and aromatic $\text{C}-\text{O}-\text{C}$ at 1280 cm^{-1}) [28–32]. This observation confirms the furan-like and oxygenated structure observed by humins synthesized from different carbohydrates [28–31].

The biocrude yield had a maximum at $250\text{ }^{\circ}\text{C}$, suggesting that its production from glucose was not favored at a higher temperature. A maximum at $280\text{ }^{\circ}\text{C}$ was also observed by Minowa et al. [20], which explained this behavior assuming the conversion of the biocrude into gas and solid. In our study, however, the biocrude yield was reduced simultaneously with an increase toward the gas phase but not toward the solid. The conversion of biocrude into other phases will be further deepened in Sect. 3.5 (*Consecutive reactions*).

To better understand their nature, the biocrude extracted from the solid (B-S) and the biocrude extracted from the aqueous phase (B-AP) were separately analyzed through GC–MS (Fig. 5). At $200\text{ }^{\circ}\text{C}$, B-S and B-AP are only constituted by furan derivatives (mostly in the form of 5-HMF and 2,5-furandicarboxaldehyde). Levoglucosan, a product of glucose dehydration [20], was also detected. As the temperature increases to $250\text{ }^{\circ}\text{C}$, the oil phases are enriched with new compounds. In particular, phenols represented the major group identified, while the portion of furanic groups decreased. The latter were no more represented by 5-HMF or similar but by benzofurans. Benzene derivatives and organic acids (levulinic acid) also appeared. At $300\text{ }^{\circ}\text{C}$, the concentration of phenols further increased, while furans were further reduced. Benzene derivatives increased and were also characterized by the presence of secondary functional groups ascribed to aldehydes and cyclic ketones. Levulinic acid was detected. At $350\text{ }^{\circ}\text{C}$, the portion of areas for benzenes and phenols additionally increased, and, with respect to the other temperature, a high quantity of cyclic ketones was identified as cyclopentenones.

In general, at all temperatures, the main differences recorded between the B-S and B-AP were due to a higher portion of phenolics in the latter, and a higher portion of benzenes in the former. This was attributed to a difference in

Fig. 4 FTIR spectra of the solids obtained with 5wt% glucose for 1 h at 250 °C (dark line) and 350 °C (red line). (The reader is referred to the web version of this paper for the color representation of this figure)



polarity, and hence in water solubility, of these two classes of compounds. In addition, other families of compounds have been found in both oil products. TGA conducted over B-S and B-AP showed that the former had a higher boiling point than the latter, while FTIR analysis showed fairly similar spectra for the two, with slightly higher intensity for the oxygenated bonds in B-AP.

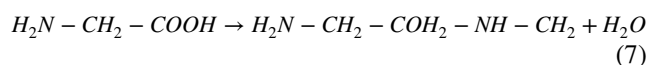
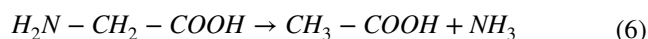
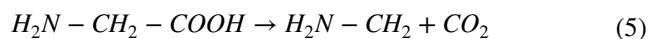
Overall, the increase in temperature involves the increase in the oil products of aromatic compounds and cyclic ketones and the decrease of furans, mainly due to the reactivity of compounds such as 5-HMF, promoters of the solid phase. The presence of the previously listed compounds in oil produced by glucose liquefaction has been documented in the literature. These include ketones and furans [16], resulting from dehydration and isomerization of glucose, and phenols, in particular the molecule 1,2,4-benzotriol (detected in B-AP at 250 °C and 300 °C), resulting from the degradation of 5-HMF [33].

3.2 Glycine

Figure 6A shows the mass yields obtained with glycine alone (GLY). At 200 °C, there is no production of phases other than the starting aqueous phase, which resulted in predominant at every temperature. Except for the aqueous phase, at 250 °C and above, the highest mass yield was observed with the gas phase. In Fig. 6B, the gas composition is reported. The gas consists mainly of CO₂ (at least 63% of the gas), in smaller amounts

of CO and H₂, and in traces by CH₄ and longer alkanes. As observed with glucose alone, the CO₂ concentration decreases with temperature while the other compounds increase. However, for each gas, including CO₂, the partial pressure, and hence the amount produced, increased with temperature.

The possible reactions that occur in hydrothermal liquefaction of amino acids are mainly decarboxylation, deamination, and dimerization [34, 35]. The formulas for these three reactions with glycine are given in Eq. 5, Eq. 6, and Eq. 7, respectively. Decarboxylation leads to the production of CO₂ and methylamine, while deamination brings to the formation of NH₃ and acetic acid. The high CO₂ concentration is hence attributable to decarboxylation. However, the CO₂ yield from direct decarboxylation was limited. In fact, the CO₂ yields according to the stoichiometry reported in Eq. 5 were relatively low: from 11.0% at 250 °C to 12.9% at 350 °C. Therefore, also because CO₂ could be produced by the degradation of other molecules coming from the glycine decomposition, as probably happened for CO and H₂, only a reduced portion of the glycine took part in the decarboxylation reaction.



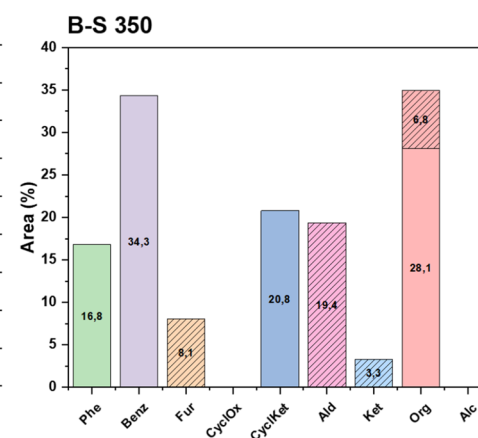
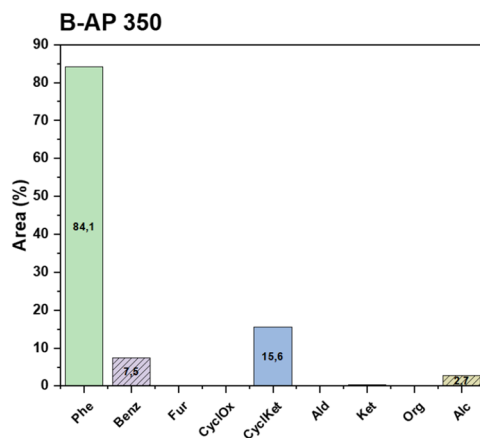
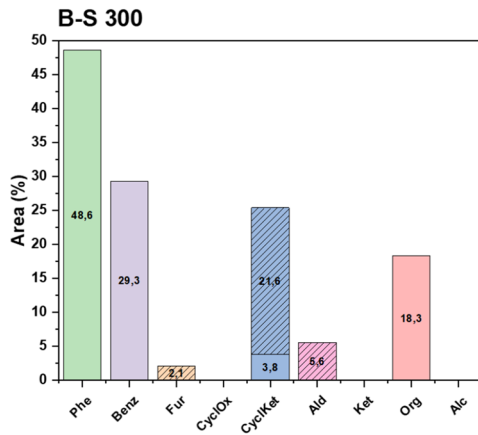
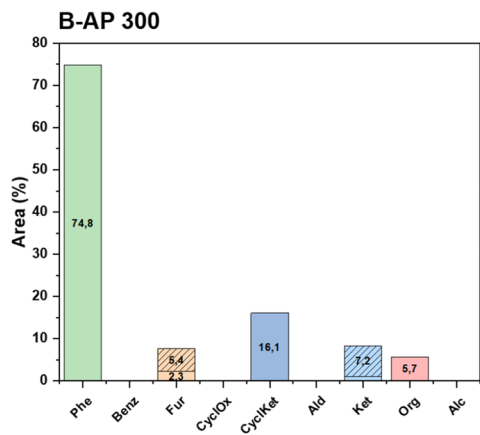
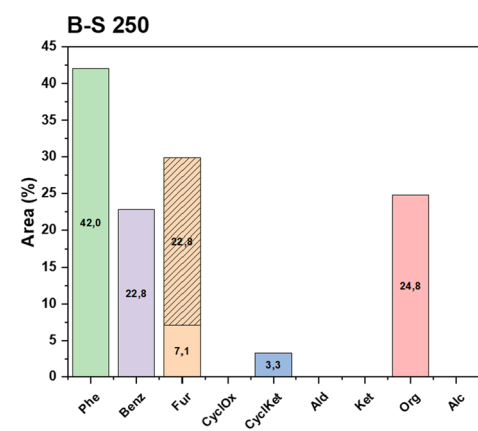
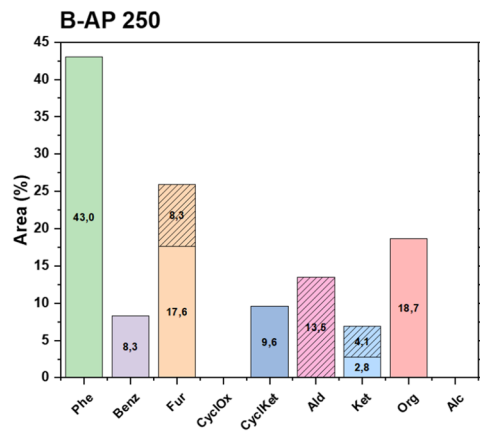
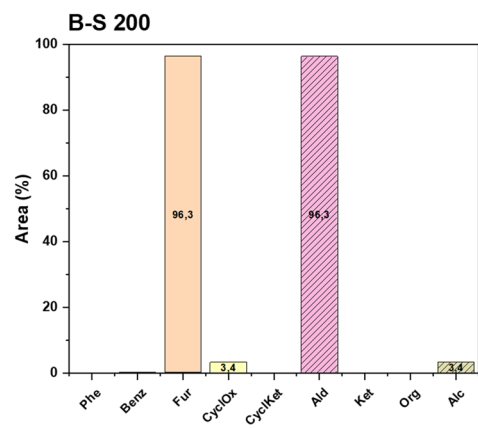
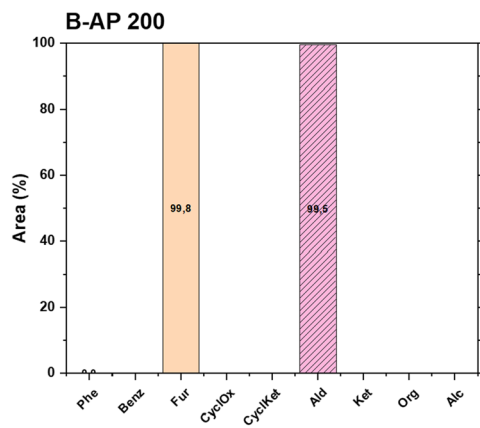


Fig. 5 Family compounds identified in the B-S and B-AP with GLU. Subdivision among: phenol derivatives (Phe), benzene derivatives (Benz), furanes (Fur), cyclic oxygenates (CyclOx), cyclic ketones (CyclKet), aldehydes (Ald), ketones (Ket), organic acids (Org), and alcohols (Alc). Bars without stripes refer to the core functional groups; striped bars refer to secondary functional groups

The solid yields were practically null while the biocrude yields were low. The biocrude consisted exclusively of B-AP and Fig. 7 shows its distributions among the different classes of compounds.

At every temperature, the highest amount of compounds belonged to the pyridine group; in particular, the main compound identified was 5-ethyl-2-methylpyridine (20 to 37% of the overall area). Pyridines are aromatic compounds having one nitrogen within a six-atom ring, as depicted in Fig. 8; their formation has been often registered as a consequence of an interaction between amino acids and decomposition products from sugars [36]. It is hence probable that pyridine formation was due to its reaction with residual compounds from its degradation. On the other hand, the formation of pyrazines was very low. Pyrazines are aromatic compounds containing two nitrogen atoms, so their formation requires the interaction between two glycine molecules. This interaction occurs through dimerization and subsequent cyclization reaction with the formation of diketopiperazines (DKPs) [13, 36, 37], which can eventually be reduced to pyrazines [38]. However, the pyrazine concentration was very low while no DKPs were detected at any temperature. This result suggests a relative insignificance of this reactive pathway. Among other nitrogen-containing aromatics, a small amount of pyrroles was detected. Benzene and phenol derivatives were also registered, often containing amino groups attached to them.

The low biocrude production from glycine alone seems to be inconsistent with what was stated by Biller and Ross [7]. In fact, they observed that biocrude has a higher yield from proteins than from carbohydrates, while in this work, glycine showed much lower biocrude than glucose reacting alone (tenfold ratio). This is probably due to the very different behavior of glycine compared with albumin and soy protein used by Biller and Ross [7]. Protein depolymerization in a hydrothermal environment is not as fast as carbohydrate depolymerization [39]. The amino acids contained in the real protein have longer and more complex side chains (e.g., phenylalanine) that, although may not be reactive, can change the solubility of the generated molecules and hence the product distribution. The partial depolymerization and decomposition of proteins would lead to shorter chains which would be constituents of the biocrude phase, resulting in a different phase distribution compared with amino acids. Therefore, the amount of biocrude from protein polymers can result in a further increase compared to the yield from glycine alone.

Glycine is the smallest amino acid, having the side chain constituted by only one hydrogen atom; it is relatively stable and is formed as a decomposition product of more complex amino acids [34]. The amino acids contained in the real protein have longer and more complex side chains (e.g., phenylalanine) that, although may not be reactive, can change the solubility of the generated molecules and hence the product distribution. However, it possesses the two functional groups (amino and carboxylic group) that characterize the chemical reactivity of all amino acids, therefore it is useful to study the general interaction with carbohydrates.

3.3 Glucose–glycine

In Fig. 9A, the mass yields for the glucose–glycine mixture (GLU–GLY) are reported. The gas yield slightly increased passing from 200 to 250 °C and then resulted constant. In contrast to the mono-component solutions, the gas phase is produced significantly already at low temperatures and it is mostly constituted by CO₂ (Fig. 9B). In fact, up to 300 °C, 99 vol.% of the gas is CO₂, and at 350 °C, only traces of other gases were detected. Moreover, the partial pressure of CO₂ remains constant from 250 °C, confirming that all CO₂ is produced at low temperatures.

The production of a substantial amount of gas at low temperatures is due to CO₂ release, which can be attributed to the Strecker degradation [40]. This reaction leads to the decarboxylation of amino acids through the oxidizing action of some sugar-derived compounds (carbonyl compounds) [41]. The amino compounds formed from Strecker degradation are considered precursors of nitrogen-containing aromatics (pyrroles, pyrazines, and pyridines among others).

The mass yield of the solid surprisingly showed a maximum yield at 250 °C (Fig. 9A). At lower temperatures, the mass yield was notable, but with increasing temperatures, the solid seems to be converted into biocrude; in fact, the biocrude yield monotonously increased with temperature (from 250 to 350 °C, it increased threefold). This hypothesis will be further investigated in Sect. 3.5 (*Consecutive reactions*). In addition, the biocrude composition is drastically different from the one registered for GLU and GLY (Fig. 10), suggesting a different behavior of the GLU–GLY mixture. At every temperature, the most abundant products observed in the oil phase are nitrogen-containing aromatics. The sum of the relative areas of these compounds goes from 97 to 80% and 71% for B-S and B-AP at 350 °C. Among these, pyrazines were widely the most present, followed by pyrroles (Fig. 10). Interestingly, the former were observed both in the B-S and in the B-AP while the latter were registered almost exclusively in the B-S. This can be probably explained by a very low aqueous solubility of pyrroles, which determines their concentration in the biocrude extracted from the solid.

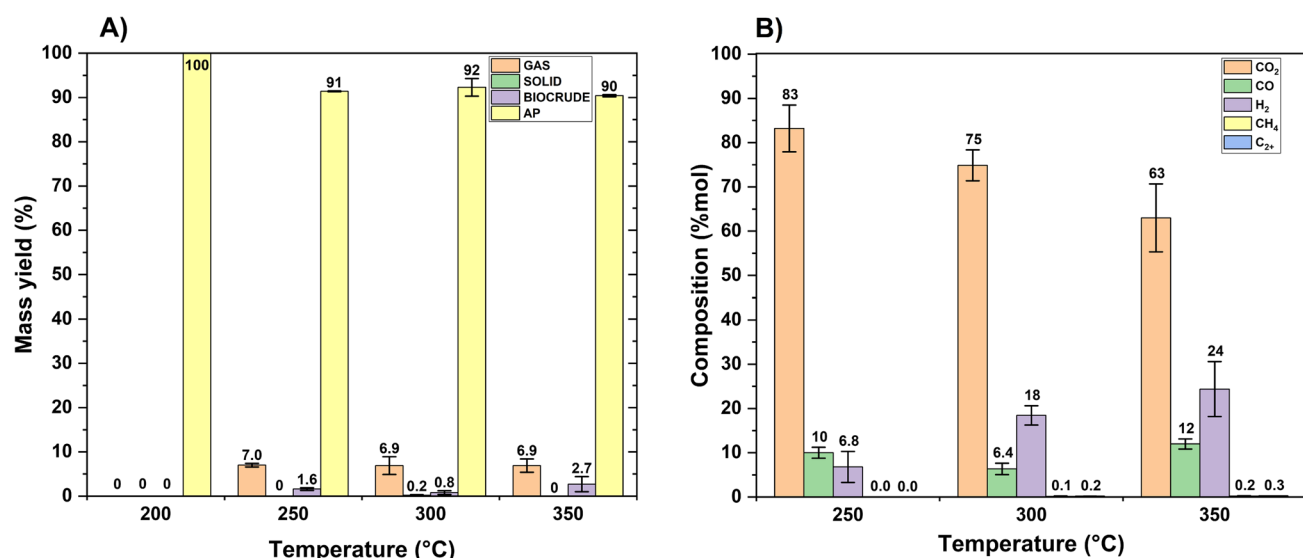


Fig. 6 **A** Mass yields with GLY at different temperatures. **B** Gas compositions (vol. %) with GLY at different temperatures. The term C₂+ is identified as ethane, ethylene, and propane. Reaction conditions: 5 wt%

glycine, 60 min, 200 g feed. (The reader is referred to the web version of this paper for the color representation of this figure)

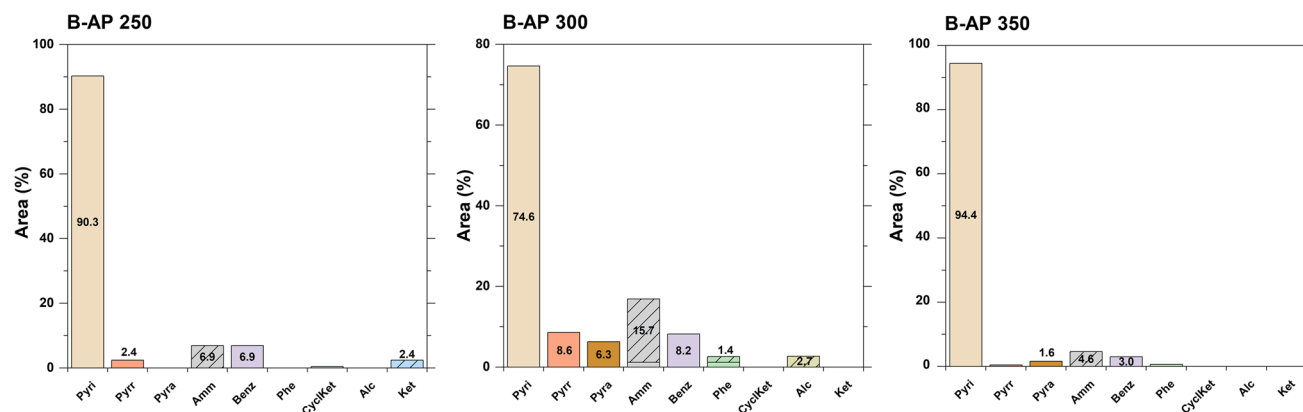


Fig. 7 Family compounds identified in the B-AP with GLY. Subdivision among pyridine derivatives (Pyri), pyrrole derivatives (Pyrr), pyrazole derivatives (Pyra), amines (Amm), benzene derivatives

(Benz), phenol derivatives (Phe), cyclic ketones (CyclKet), alcohols (Alc), and ketones (Ket). Bars without stripes refer to the core functional group; striped bars refer to secondary functional groups

Pyrazines have been identified in the literature as a product of the degradation of intermediates of the Maillard reaction [42]. The Maillard reaction is an intricate set of reactions, including the Strecker degradation, that is initially ascribed to the interaction between amino groups (coming from ammonia, amino acids, or amines) and carbonyl groups (coming from reductive sugars or their aldol-splitting derivatives) [8]. The products are called Amadori compounds, which in the second stage lead to the formation of melanoidins. These are high molecular weight compounds known for their characteristic brown color and for their solubility in water and insolubility in diethyl ether [43]. The glucose-amino acid system is known to be affected by this pathway [8, 43, 44] and the high presence of pyrazines, as well as pyrroles, confirmed this theory [45].

At low temperatures, only pyrazines and pyrroles were detected, as well as pyridinol (pyrazines with one oxydril group derived from the Maillard reaction [43]) and a few cyclic ketones. Increasing to 250 °C and 300 °C, other compounds also appeared, namely indoles, amino groups, phenols, and benzene derivatives. Indoles are usually identified in biocrude obtained from real protein-alone feedstock [9, 11, 46], but in this work, they were not observed from GLY; this could be explained by different reaction mechanisms between glycine and real proteins. Amino groups were mainly found as substituents attached to phenols or in the form of pyrrolidines. Phenols and benzenes were almost always observed with amine groups attached, suggesting a different formation pathway with respect to benzenes and phenols registered for glucose alone. Finally, at 350 °C,

Fig. 8 Nitrogen-containing aromatics identified in this work. The yellow and green dashed groups contain the most occurring molecules identified with glycine alone and glucose–glycine, respectively

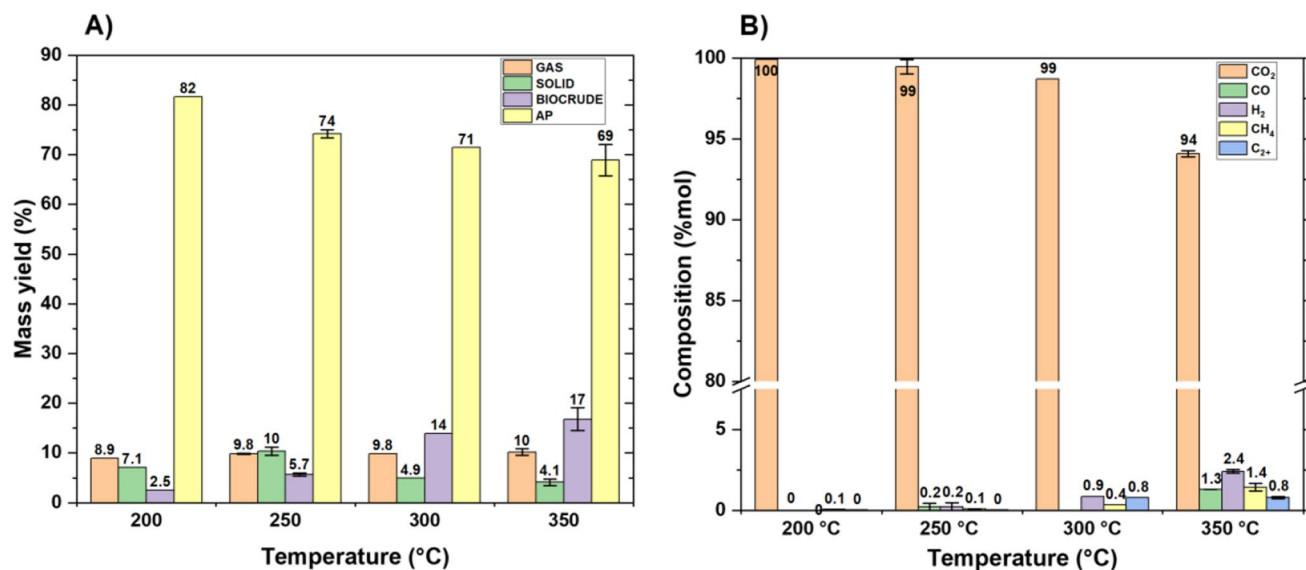
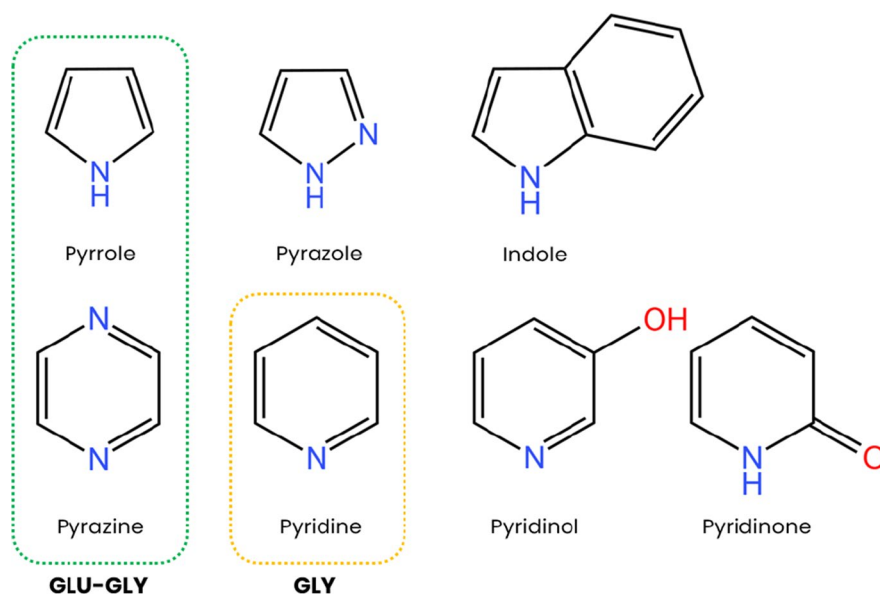


Fig. 9 **A** Mass yields with GLU-GLY at different temperatures. **B** Gas compositions (vol. %) with GLU-GLY at different temperatures. The term C2+ is identified as ethane, ethylene, and propane. Reaction

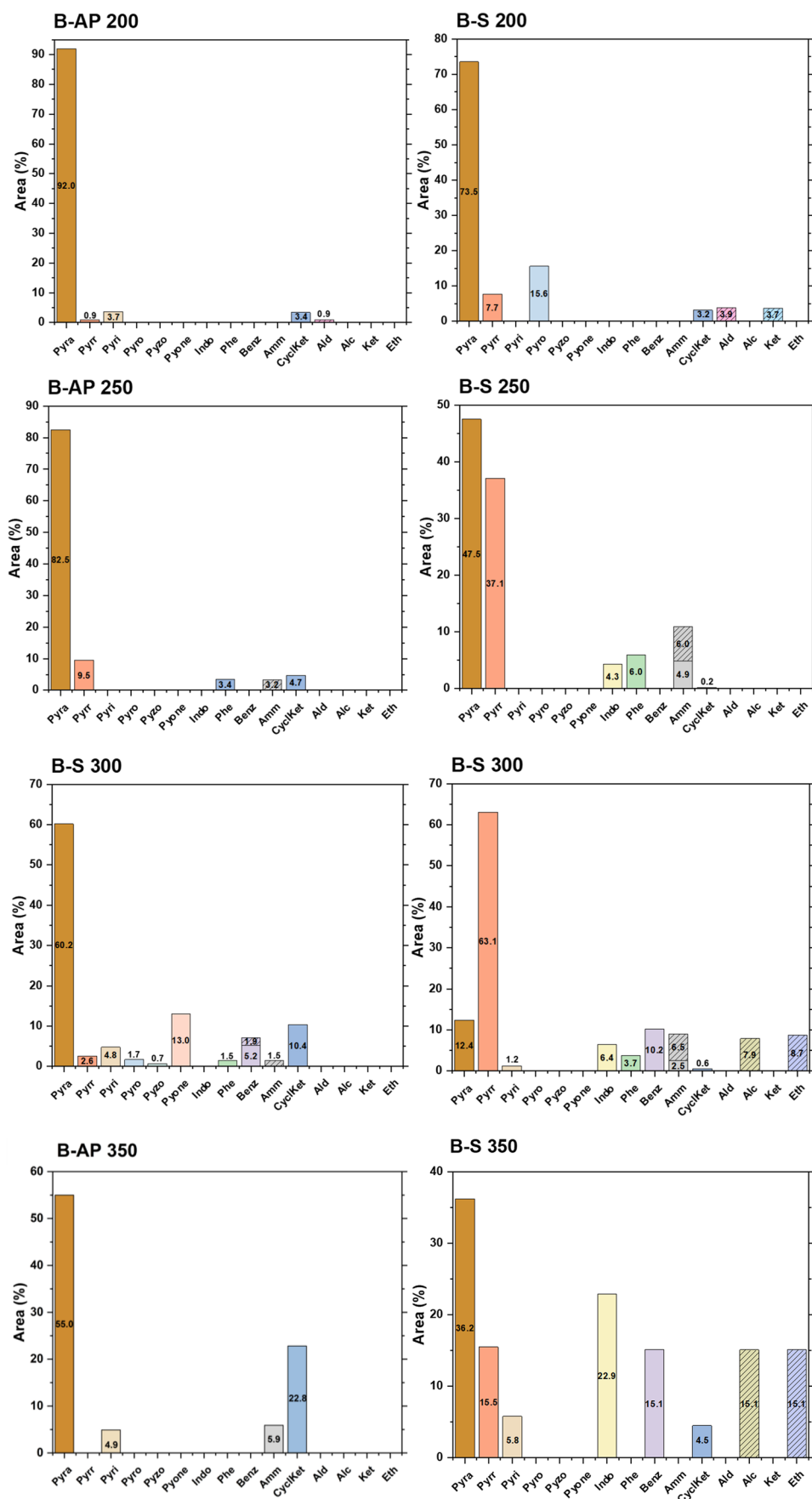
conditions: 5 wt% glucose, 5 wt% glycine, 60 min, 200 g feed. (The reader is referred to the web version of this paper for the color representation of this figure)

cyclic ketones (mainly in the form of cyclopentenones), as well as indoles, pyridines, and benzenes, increased further.

As was described for the biocrude yield and composition, the co-presence of glycine strongly modified the reactions to which glucose was subjected. This was also confirmed by the analysis of the aqueous phase composition (Supplementary Figure S2). For clarity, it is reiterated that nitrogen-containing compounds are not reported. The main compounds identified were organic acids (mainly propionic and butanoic acid) as well as alcohols (methanol and ethanol) derived from acid dehydrolysis

[36]. Acetic acid was observed at all temperatures in carbon yields ranging from 2.4 to 3.0% and its formation could be attributable to glycine deamination or glucose decomposition. Compounds such as levulinic acid, formic acid, and 5-HMF, due to the decomposition of glucose and previously observed as predominant with glucose alone, showed lower carbon yields with GLU-GLY (taking into account also the different carbon distribution in the feedstock with GLU and GLU-GLY). This indicates a strong interaction of glycine with glucose degradation pathways, as previously observed by Peterson et al. [8].

Fig. 10 Family compounds identified in the B-S and B-AP with glucose–glycine. Subdivision among pyrazine derivatives (Pyra), pyrrole derivatives (Pyrr), pyridine derivatives (Pyri), pyridinol derivatives (Pyro), pyrazole derivatives (Pyzo), pyridinone derivatives (Pyone), indoles (Indo), amines (Amm), benzene derivatives (Benz), phenol derivatives (Phe), cyclic ketones (CyclKet), alcohols (Alc), ketones (Ket), and ethers (Eth). Bars without stripes refer to the core functional group; striped bars refer to secondary functional groups



3.4 Glucose–glycine interaction

To better study the interaction between glucose and glycine, in Fig. 11, the absolute (A) and relative (B) differences between the mass yields obtained experimentally and those obtained as an average of the performance of the individual monomers are shown. In both figures, a positive value represents an increase in mass yield with the co-presence of both molecules (synergy), while a negative value represents a decrease (antagonism).

At low temperatures, with the GLU-GLY system, the gas yield is considerably favored compared to the monomers alone (Fig. 11B). Looking at the differences between the partial pressure of GLU-GLY and the sum of those of GLU and GLY (Supplementary Figure S3), it is clear that already at 200 °C the co-presence of the two led to the production of a high amount of CO₂ that, as previously described, can be attributed to the Strecker degradation. The synergy towards the gas formation however decreased with an increase in temperature. This is partially due to the increase in the gas production with the monomers, as well as a substantial non-variation of the gas from GLU-GLY at higher temperatures (Fig. 9A). In addition, at every temperature, GLU-GLY produces a lower amount of CO and H₂ and these differences are enlarged as temperature increases. These gases can be traced to degradation mechanisms of unstable products at high temperatures, the formation of which thus appears to be limited for GLU-GLY.

The strong interaction between glucose and glycine can be easily observed from the behaviors of solid and biocrude (Fig. 11). The solid was favored at 200 °C while

became disfavored as temperature increased. In contrast, the biocrude formation showed an opposite trend: at 200 °C it was reduced while at 350 °C was increased by 93% (on a relative basis). This suggests a strong correlation and interchange between biocrude and solid. At 200 °C, glucose and glycine are already reacting with each other, leading to the formation of a solid phase and to the reduction of the already limited biocrude formation that would take place with GLU. The interaction between the two molecules has been previously studied in the literature at low temperatures. The reaction mechanisms have generally been traced back to the Maillard reaction [8, 47] and Strecker degradation [40, 41], with the latter that can be included within the former. The Maillard reaction involves the formation of melanoidins from which the biocrude is formed. However, melanoidins are water-soluble compounds which are hence present in the aqueous phase. They have been mainly studied in the literature after freeze-drying of the aqueous phase [40, 43, 48]. Fang et al. [40] saw that the solid fraction generated from glucose and glycine has similar ¹³C and ¹⁵N NMR spectra to those of the melanoidin fraction suggesting a possible similar nature between solid and melanoidins. For this reason, the increase in temperature could have led to the degradation of the solid with a consequent increase in the biocrude formation. On the other hand, with GLU, the solid formation should be ascribed to the formation of the humins, which showed more stability and did not seem to be precursors of the biocrude formation. These hypotheses were tested through consecutive tests presented in Sect. 3.5 (*Consecutive reactions*).

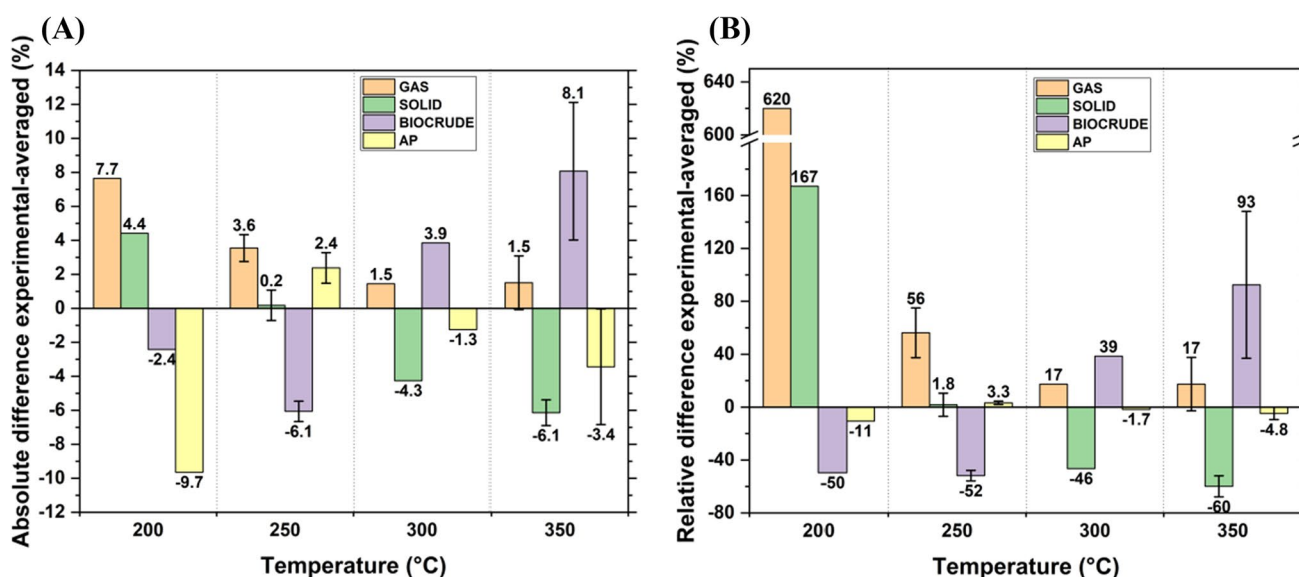


Fig. 11 Absolute (A) and relative (B) differences between experimental mass yields of GLU-GLY and mass-averaged yields for GLU and GLY. (The reader is referred to the web version of this paper for the color representation of this figure)

3.5 Consecutive reactions

3.5.1 Evolution of the phases

To further investigate the relationships between the phases, a campaign of consecutive tests was carried out. Except for the gas phase, the products generated from GLU and GLU-GLY obtained at 250 °C were separated and then used as reactants for a second reaction at 350 °C for 1 h. The temperature of 250 °C was chosen for the first step because it led to the maximum yield in biocrude for GLU and the maximum yield in solid for GLU-GLY; analysis of the products generated by these phases could highlight how their formation is correlated. In Fig. 12 and Fig. 13, the phase distribution for the consecutive test campaign is reported for GLU and GLU-GLY, respectively.

Looking at the gas phase, although the mass yield is similar between GLU and GLU-GLY at 350 °C, it is easy to see that it derives from two different pathways. With GLU at 350 °C, the gas clearly increased due to contributions from all the phases, while with GLU-GLY, it remained similar to the yield at 250 °C. With GLU, the increase in gas is not attributable only to the organics in the aqueous phase, as would be expected, but also to large contributions from solid and biocrude. These phases produced different gas compositions; Figure S4 shows the composition of the gas (averaged) at 350 °C, highlighting the contribution of each phase. The solid produced mainly CO₂, suggesting its decomposition through decarboxylation reactions; the aqueous phase contributed largely to the

H₂ production, probably due to formic acid decomposition, as well as CO₂; the biocrude led to the formation of CO₂ and to a consistent amount of H₂ and CH₄. The formation of the latter two therefore occurs according to more complex mechanisms than just decarboxylation. In addition, the gas distribution appears to be slightly different from the products generated at 350 °C for 1 h, due to a decrease in CO in favor of H₂.

As previously described, gas production with GLU-GLY started at 200–250 °C and then remained approximately constant. Therefore, the solid, biocrude, and aqueous phases decomposed only to a very limited extent into gaseous products at higher temperatures. A small contribution came mainly from the solid as CO₂ while the H₂ registered at 350 °C was mostly attributable to compounds in the aqueous phase (Figure S5).

The biggest differences between GLU and GLU-GLY were observed with the trends of the formation of solid and biocrude phases. With GLU, the solid decreased from 250 to 350 °C, but most of the solid remained as such, with a smaller portion converted into water-soluble compounds and gas, while a negligible fraction was converted into biocrude, whose yield remained constant overall. In fact, this apparent stability was the result of a positive contribution (conversion of some water-soluble in biocrude) and a negative contribution (conversion of biocrude into aqueous products, gas and solid).

With GLU, looking at the composition of the biocrude formed at 350 °C from the biocrude generated at 250 °C, it resulted in a higher concentration of benzene-derived

Fig. 12 Sankey diagram with product distributions at 250 °C for GLU and for consecutive reactions of single phases reacting alone at 350 °C. All consecutive reactions were performed in duplicates

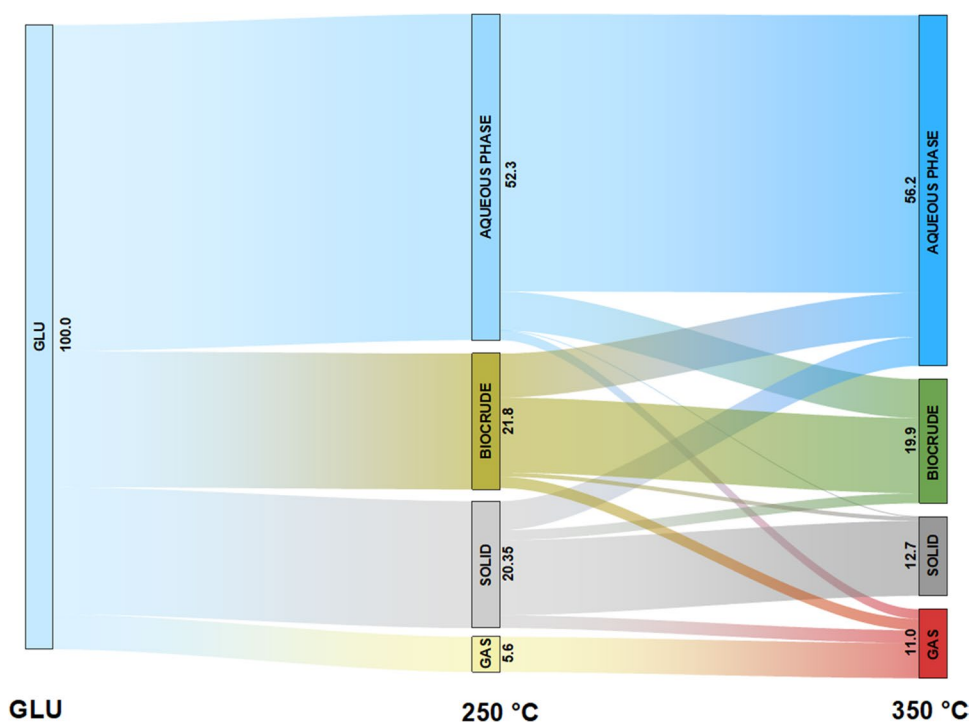
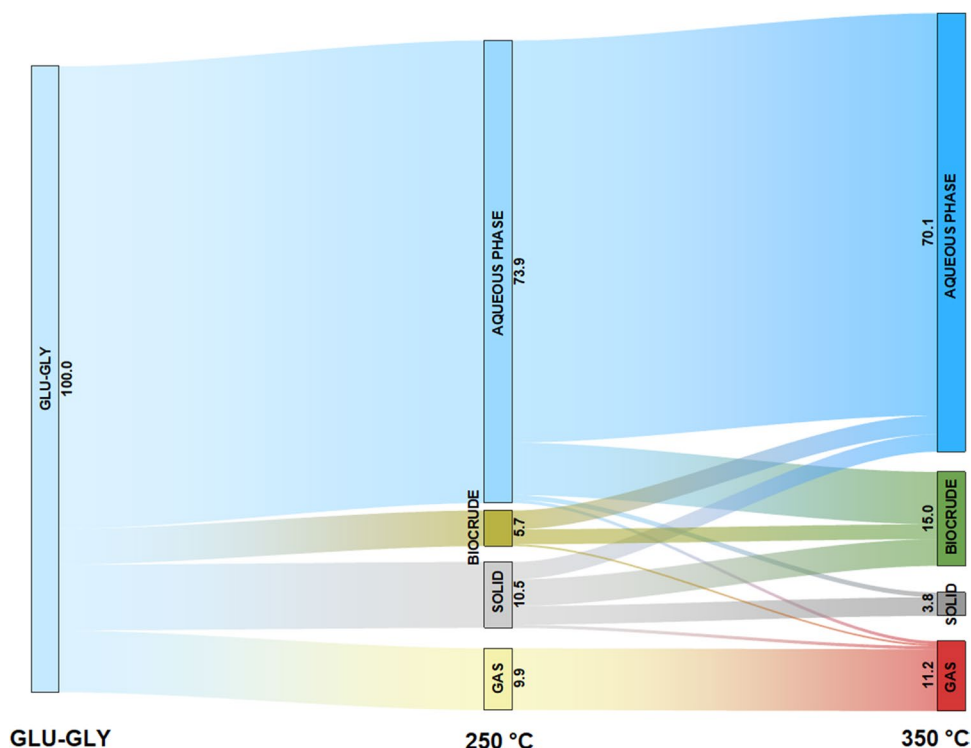


Fig. 13 Sankey diagram with product distributions at 250 °C for GLU-GLY and for consecutive reactions of single phases reacting alone at 350 °C. All consecutive reactions were performed in duplicates



compounds, mainly in the form of benzofuranones, indanones, and indenones and a lower concentration of benzofurans, suggesting their conversion to the aforementioned compounds. The water-soluble compounds contained in the aqueous phase produced at 350 °C a biocrude phase rich in benzenes (ca. 35%) and phenols (ca. 25%). Overall, the biocrudes obtained from the consecutive tests (from biocrude and aqueous phase) were found to be very similar to those obtained with GLU at 350 °C for 1 h (Fig. 5). For this reason, it is corroborated that for GLU, the biocrude formation also occurs from compounds present in the aqueous phase. Moreover, the solid production from biocrude was almost null, while the production of compounds released in the aqueous phase and gas was consistent. This suggests that biocrude does not undergo recombination reactions that promote char formation, but rather degradation mechanisms that lead to the formation of gas and aqueous phase products.

Looking at GLU-GLY (Fig. 13), the mechanisms present are different, in particular, the solid dramatically decreased from 250 to 350 °C, as seen also in Fig. 3. Confirming the hypothesis made above, it is clear from Fig. 13 that the majority of the solid phase (41 wt% of the solid generated in the first step) was converted to biocrude. Analyzing the biocrude obtained from the solid, the compounds found in the B-AP were mostly pyrazines-derivatives (57% of the overall integrated area), confirming a composition similar to the biocrude at 250 °C for 1 and 350 °C for 1 h. On the other hand, in the B-S, which constituted 56% of the biocrude

phase, most of the compounds were represented by indole-derivatives (74% of the overall integrated area). These molecules were found in lower concentration in GLU-GLY at 350 °C; it is then possible that the appearance of indoles at high temperatures is due to the degradation of the solid. In general, these observations justify the assumption that the solid is an intermediate for the biocrude production with GLU-GLY, contrary to the idea that the solid constitutes an end product of the HTL reaction [6, 49]. The intermediate behavior herein observed can be attributed to the thermal instability of the solid phase, having a melanoidin-like structure with high molecular weight. To exclude a kinetic limitation for the conversion of the solid into biocrude, a longer test at 250 °C and 6 h was also performed. Compared with 250 °C for 1 h, the mass yield resulted higher for the solid (12 wt%), for the biocrude (8.5 wt%), but lower for the aqueous phase (70 wt%). Solid decomposition was hence driven by the higher reaction temperature rather than the longer residence time used in the consecutive reactions.

The aqueous phase gave the highest contribution to the biocrude formation (8.4 wt% of the starting feed). This is in agreement with the idea that melanoidins are formed in the presence of glucose and glycine and that these are intermediate in the formation of biocrude. As seen for GLU, also with GLU-GLY, a fraction of the biocrude was converted to aqueous phase-soluble. Furthermore, solid seemed not to be formed from biocrude, as assumed also from Minowa et al. [10], despite a carbonization process would be expected for a long reaction time.

3.5.2 Interaction between the phases

The consecutive reactions were designed in order to understand how the phases produced at 250 °C (1 h) for GLU and GLU-GLY were related to the reaction at 350 °C (1 h), and the results are depicted in Fig. 14 (please note that the figure contains also data reported in the above paragraphs to facilitate the comparison). With regards to GLU (Fig. 14, left), it is interesting to note that the yields obtained as a linear combination of the consecutive reactions (yellow bars) did not correspond with the yields obtained at 350 °C (cyan bars). In particular, the difference was strong for solid and biocrude. On the other hand, with GLU-GLY (Fig. 14, right), the mass yields as a linear combination of the consecutive reactions were very similar to those at 350 °C for 1 h.

To understand whether the differences were due to the different thermal profiles used (350 °C for 1 h versus 250 °C for 1 h + 350 °C for 1 h) or to the fact that some phase interactions were hindered by phase separation before the second step, an additional test was designed. That is, after an initial reaction at 250 °C for 1 h, the reactor was cooled down and the gas phase was removed without opening the reactor. Then, the reactor was re-inerted, pressurized to 3 bar, and raised to 350 °C for 1 h without prior separation of the solid and liquid phases. In Fig. 14, the resulting mass yields are reported as “non-isolated,” in orange bars. (The reader is referred to the web version of this paper for the color representation of this figure).

Comparing the non-isolated test (orange bars) with the results obtained at 350 °C for 1 h (cyan bars), it can be easily seen that the mass yields are remarkably similar, except for the gas phase, with both GLU and GLU-GLY. This similarity suggests that the higher residence time used in

the consecutive steps (1 h at 250 °C + 1 h at 350 °C) with respect to the reaction at 350 °C (1 h) did not affect that much the final distribution among the phases. The only difference recorded on the gas phase can be explained by the fact that the removal of the gas phase after the first step (1 h at 250 °C) favored the gas production in the second step. For this reason, some equilibrium limitations for gas production are possible.

Comparing the mass yields in the isolated tests (yellow bars) with those non-isolated, GLU and GLU-GLY showed different behaviors. In fact, with the latter, the yields of solid, biocrude, and AP were always fairly similar, so it is possible to assume that with GLU-GLY no interactions between the phases were registered. On the other hand, with GLU, the solid production was favored and the biocrude production disfavored by the co-presence of all the phases. It is hence probable that some kind of equilibrium-limited interactions took place among the different phases, whereby the separation of these leads to a different distribution of final products. For example, Liu et al. [50] proposed a solid formation mechanism from humins (i.e., the solid phase derived from the hydrothermal conversion of glucose) in which an equilibrium between polymerization and depolymerization reactions is involved. Therefore, we may suggest that the solid formed during the first step, successively being in contact with clean water during the second step, undergoes depolymerization, since the water does not contain any of its precursors. Additional investigation is encouraged to better understand this phenomenon. This interaction was further confirmed by testing the three phases recovered from the first step with glucose (solid, biocrude, and aqueous phase) in combination with each other at 350 °C for 1 h (Figure S6). All the combinations

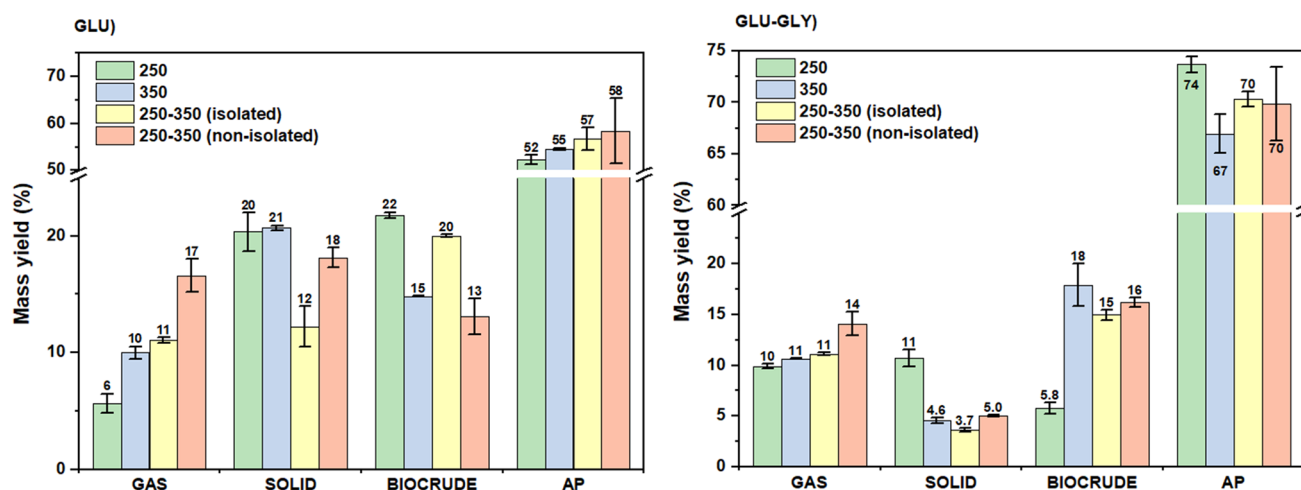


Fig. 14 Mass yields at 250 °C for 1 h (green, 250), 350 °C for 1 h (cyan, 350), 250 °C for 1 h + 350 °C for 1 h separating the phases (yellow, 250–350 (isolated)), and 250 °C for 1 h + 350 °C for 1 h without separating the phases (orange, 250–350 (non-isolated)).

GLU on the left, GLU-GLY on the right. With 250–350 (isolated) and 250–350 (non-isolated), the gas yield takes into account the gas formed after the first step plus the gas formed in the second step

tested (aqueous phase + solid, aqueous phase + biocrude, and solid + biocrude in freshwater) showed a synergy towards the solid and aqueous phase and an antagonism towards the biocrude. Moreover, observing the linear combinations of the mass yields obtained with the biphasic reaction (Figure S7, grey), it can be easily seen that solid and biocrude resembled quite well the results obtained without isolation of the phases (Figure S7, orange). It is then corroborated by the hypothesis that with glucose there are strong interactions among the phases themselves that characterize the final distribution of the phases.

3.6 Mechanism description

Figure 15 depicts the relationships between the phases observed for GLU reacting alone. Glucose is converted into a plethora of organic compounds soluble in the aqueous phase; among these, 5-HMF is formed by isomerization-dehydration and is the intermediate for the formation of the solid phase and biocrude. Already at low temperatures, 5-HMF reacts with levulinic acid, its dehydration product, or with itself to produce an oligomeric structure (humins) that constituted the solid phase. Humins are in a kind of polymerization/depolymerization equilibrium with the aqueous compounds. Despite the presence of furan groups in the chemical structure of humins, which might suggest their conversion into biocrude-soluble compounds, a very limited transformation of the solid into biocrude was observed. On the contrary, biocrude formation is likely to occur from 5-HMF, aldehydes, and ketones. The biocrude

is then degraded at higher temperatures into water-soluble. The gas phase is formed at both low and high temperatures and from all other phases. CO_2 is the main gaseous product formed and derives from AP, solid, and biocrude, probably mainly from decarboxylation reactions. CO and H_2 are also produced from the AP, the latter likely from formic acid, while a few CH_4 is formed from biocrude through demethylation.

Figure 16 displays the phase relationships observed for glucose and glycine reacting together (GLU-GLY). These two molecules show a strong interaction already at very low temperatures due to the reaction between the amino group of the amino acid and the carbonyl group of the monosaccharide. This leads to the formation of Amadori compounds, which are intermediates in the Maillard reaction. Among the various chemical pathways that occur during the Maillard reaction, there is Strecker degradation, which results in the release of CO_2 . The only gas formed in the co-presence of glucose and glycine is CO_2 that is formed at low temperatures through this mechanism. From the Maillard reaction, melanoidins are produced. Melanoidins are molecules known to have a very high molecular weight and to be water-soluble. Simultaneously with melanoidins, a solid phase with a structure similar to melanoidins is also produced. Both the melanoidins in the aqueous phase and the solid are precursors of the biocrude phase. At high temperatures, these structures are indeed thermally degraded into nitrogen-containing aromatics, mainly pyrazines and pyridines, which constitute the biocrude.

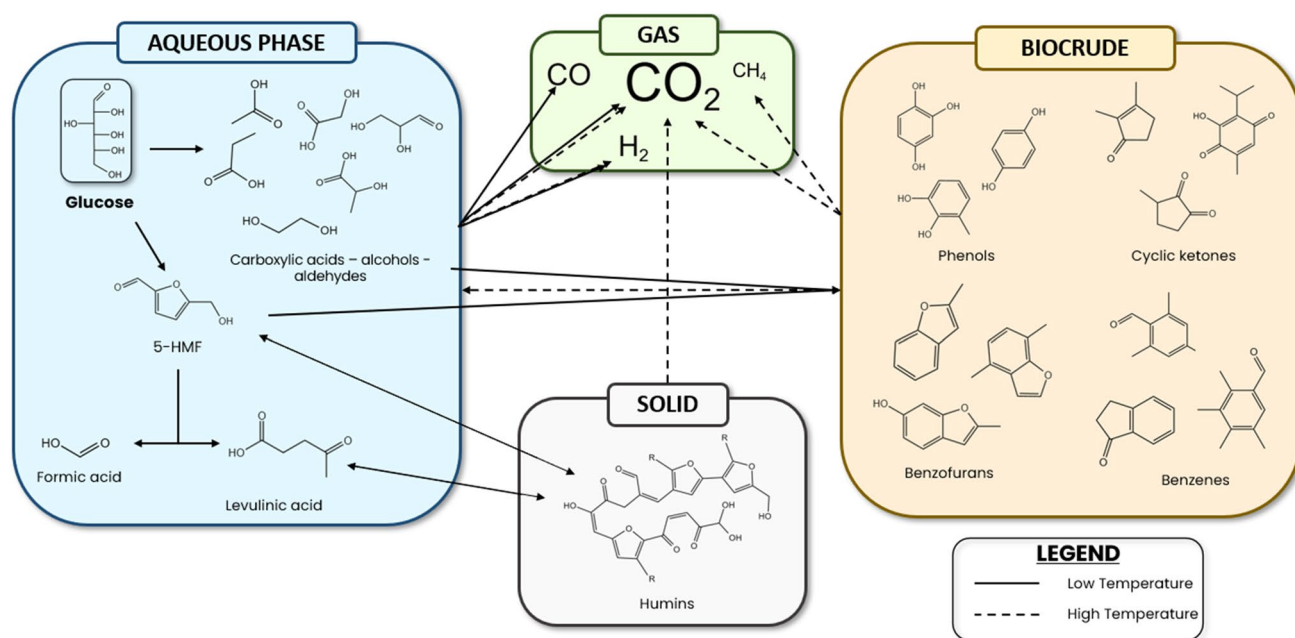


Fig. 15 Suggested interchange mechanisms among phases with glucose (GLU)

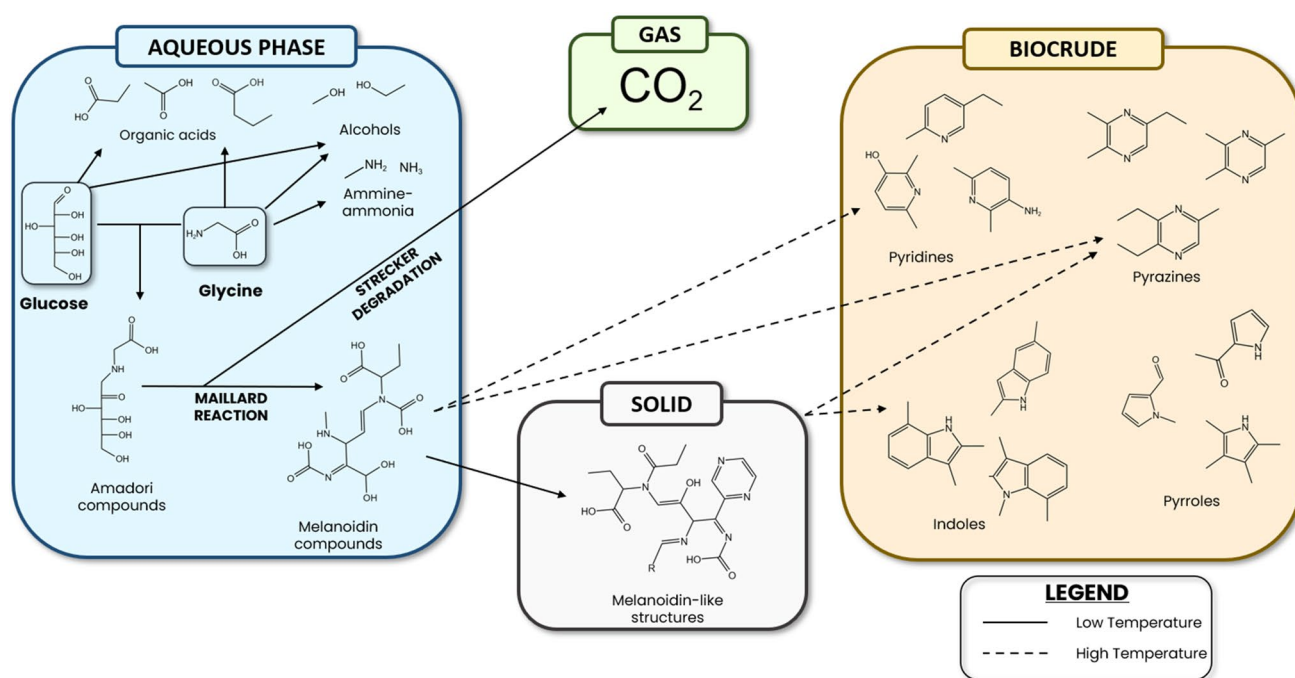


Fig. 16 Suggested interchange mechanisms among phases with glucose and glycine (GLU-GLY)

4 Conclusions

The interaction between carbohydrates and proteins during hydrothermal liquefaction has been investigated at different temperatures by experimental tests with glucose and glycine. The study was performed by comparing the reactivity of these two molecules alone or in combination, as well as by observing the reaction pathways activated by each different phase produced in such HTL tests. The results have shown a strong interaction between glucose and glycine resulting in a set of products that differed significantly from the simple overlapping of the single monomer reactivities. In particular, solid and biocrude phases are strongly correlated. In fact, in contrast to the mechanisms occurring with glucose alone, the co-presence of glucose and glycine leads to higher solid and lower biocrude productions at low temperatures (250 °C) and the opposite at higher temperatures (350 °C). With remarkable novelty with respect to literature, consecutive reactions involving the generated phases have been performed to deepen the interchange phenomena. With glucose–glycine reacting together, solid and aqueous phase residues obtained at low temperatures convert at high temperatures into biocrude. Finally, with glucose alone, the co-presence of solid and liquid phases (biocrude and aqueous residues) has a synergistic tendency towards the biocrude production at the expense of the gas and solid phase. Overall, this work strengthens the hypothesis that carbohydrates and proteins have a robust interaction during hydrothermal

liquefaction, highlighting the central role of temperature in regulating such interaction. Furthermore, the experimental observations of interchange between the different phases of HTL allowed an understanding of the production/conversion of each phase and hence a better tuning of the reaction conditions towards the product of interest.

Supplementary Information The online version contains supplementary material available at <https://doi.org/10.1007/s13399-023-03967-7>.

Author contribution Edoardo Tito: data curation; formal analysis; investigation; methodology; writing—review and editing. Giuseppe Pipitone: data curation; formal analysis; methodology; supervision; writing—review and editing. Alessandro H.A. Monteverde Videla: conceptualization; supervision. Samir Bensaid: conceptualization, project administration; supervision; writing—review and editing. Raffaele Pirone: conceptualization, project administration; supervision; writing—review and editing.

Funding Open access funding provided by Politecnico di Torino within the CRUI-CARE Agreement.

Data availability The data set is available from the corresponding author on realistic demand.

Code availability Not applicable.

Declarations

Ethics approval The authors declare that the manuscript has not been published previously.

Consent to participate Not applicable.

Consent for publication Not applicable.

Competing interests The authors declare no competing interests.

Open Access This article is licensed under a Creative Commons Attribution 4.0 International License, which permits use, sharing, adaptation, distribution and reproduction in any medium or format, as long as you give appropriate credit to the original author(s) and the source, provide a link to the Creative Commons licence, and indicate if changes were made. The images or other third party material in this article are included in the article's Creative Commons licence, unless indicated otherwise in a credit line to the material. If material is not included in the article's Creative Commons licence and your intended use is not permitted by statutory regulation or exceeds the permitted use, you will need to obtain permission directly from the copyright holder. To view a copy of this licence, visit <http://creativecommons.org/licenses/by/4.0/>.

References

- Mathanker A, Das S, Pudasainee D, Khan M, Kumar A, Gupta R (2021) A review of hydrothermal liquefaction of biomass for biofuels production with a special focus on the effect of process parameters, co-solvents and extraction solvents. *Energies* 14:4916. <https://doi.org/10.3390/en14164916>
- Mishra RK, Kumar V, Kumar P, Mohanty K (2022) Hydrothermal liquefaction of biomass for bio-crude production: a review on feedstocks, chemical compositions, operating parameters, reaction kinetics, techno-economic study, and life cycle assessment. *Fuel* 316:123377. <https://doi.org/10.1016/j.fuel.2022.123377>
- Toor SS, Rosendahl L, Rudolf A (2011) Hydrothermal liquefaction of biomass: a review of subcritical water technologies. *Energy* 36:2328–2342. <https://doi.org/10.1016/j.energy.2011.03.013>
- Akiya N, Savage PE (2002) Roles of water for chemical reactions in high-temperature water. *Chem Rev* 102:2725–2750. <https://doi.org/10.1021/cr000668w>
- Peterson AA, Vogel F, Lachance RP, Fröling M, Antal MJ, Tester JW (2008) Thermochemical biofuel production in hydrothermal media: a review of sub- and supercritical water technologies. *Energy Environ Sci* 1:32–65. <https://doi.org/10.1039/b810100k>
- Gollakota ARK, Kishore N, Gu S (2018) A review on hydrothermal liquefaction of biomass. *Renew Sustain Energy Rev* 81:1378–1392. <https://doi.org/10.1016/j.rser.2017.05.178>
- Biller P, Ross AB (2011) Potential yields and properties of oil from the hydrothermal liquefaction of microalgae with different biochemical content. *Bioresour Technol* 102:215–225. <https://doi.org/10.1016/j.biortech.2010.06.028>
- Peterson AA, Lachance RP, Tester JW (2010) Kinetic evidence of the maillard reaction in hydrothermal biomass processing: glucose-glycine interactions in high-temperature, high-pressure water. *Ind Eng Chem Res* 49:2107–2117. <https://doi.org/10.1021/ie9014809>
- Changi SM, Faeth JL, Mo N, Savage PE (2015) Hydrothermal reactions of biomolecules relevant for microalgae liquefaction. *Ind Eng Chem Res* 54:11733–11758. <https://doi.org/10.1021/acs.iecr.5b02771>
- Minowa T, Inoue S, Hanaoka T, Matsumura Y (2004) Hydrothermal reaction of glucose and glycine as model compounds of biomass. *Nihon Enerugi Gakkaishi/Journal Japan Inst Energy* 83:794–798. <https://doi.org/10.3775/jie.83.794>
- Teri G, Luo L, Savage PE (2014) Hydrothermal treatment of protein, polysaccharide, and lipids alone and in mixtures. *Energy Fuels* 28:7501–7509. <https://doi.org/10.1021/ef501760d>
- Fan Y, Hornung U, Dahmen N, Kruse A (2018) Hydrothermal liquefaction of protein-containing biomass: study of model compounds for Maillard reactions. *Biomass Convers Biorefinery* 8:909–923. <https://doi.org/10.1007/s13399-018-0340-8>
- Zhang C, Tang X, Sheng L, Yang X (2016) Enhancing the performance of Co-hydrothermal liquefaction for mixed algae strains by the Maillard reaction. vol. 18. <https://doi.org/10.1039/c5gc02953h>
- Dénier M, Haarlemmer G, Roubaud A, Weiss-Hortala E, Fages J (2017) Hydrothermal liquefaction of blackcurrant pomace and model molecules: understanding of reaction mechanisms. *Sustain Energy Fuels* 1:555–582. <https://doi.org/10.1039/c6se00065g>
- Lu J, Liu Z, Zhang Y, Savage PE (2018) Synergistic and antagonistic interactions during hydrothermal liquefaction of soybean oil, soy protein, cellulose, xylose, and lignin. *ACS Sustain Chem Eng* 6:14501–14509. <https://doi.org/10.1021/acssuschemeng.8b03156>
- Lu J, Fan G, Yang M, Wu Y (2022) Origin of carbon in the bio-oil from hydrothermal liquefaction of protein and glucose via isotopic labeling. *Fuel* 308:121941. <https://doi.org/10.1016/j.fuel.2021.121941>
- Sheehan JD, Savage PE (2017) Molecular and lumped products from hydrothermal liquefaction of bovine serum albumin. *ACS Sustain Chem Eng* 5:10967–10975. <https://doi.org/10.1021/acssuschemeng.7b02854>
- Gautam R, Vinu R (2020) Reaction engineering and kinetics of algae conversion to biofuels and chemicals: via pyrolysis and hydrothermal liquefaction. vol. 5. <https://doi.org/10.1039/d0re00084a>
- Obeid R, Lewis DM, Smith N, Hall T, van Eyk P (2020) Reaction kinetics and characterisation of species in renewable crude from hydrothermal liquefaction of monomers to represent organic fractions of biomass feedstocks. *Chem Eng J* 389:124397. <https://doi.org/10.1016/j.cej.2020.124397>
- Minowa T, Fang Z, Ogi T, Várhegyi G (1998) Decomposition of cellulose and glucose in hot-compressed water under catalyst-free conditions. *J Chem Eng Japan* 31:131–134. <https://doi.org/10.1252/jcej.31.131>
- Promdej C, Matsumura Y (2011) Temperature effect on hydrothermal decomposition of glucose in sub- and supercritical water. *Ind Eng Chem Res* 50:8492–8497. <https://doi.org/10.1021/ie200298c>
- Kruse A, Krupka A, Schwarzkopf V, Gamard C, Henningsen T (2005) Influence of proteins on the hydrothermal gasification and liquefaction of biomass 1 Comparison of different feedstocks. *Ind Eng Chem Res* 44:3013–20. <https://doi.org/10.1021/ie049129y>
- Kabyemela BM, Adschiri T, Malaluan RM, Arai K (1999) Glucose and fructose decomposition in subcritical and supercritical water: detailed reaction pathway, mechanisms, and kinetics. *Ind Eng Chem Res* 38:2888–2895. <https://doi.org/10.1021/ie9806390>
- Gomes FNDC, Pereira LR, Ribeiro NFP, Souza MMVM (2015) Production of 5-hydroxymethylfurfural (HMF) via fructose dehydration: effect of solvent and salting-out. *Brazilian J Chem Eng* 32:119–126. <https://doi.org/10.1590/0104-6632.20150321s0002914>
- Jakob A, Grilc M, Teržan J, Likozar B (2021) Solubility temperature dependence of bio-based levulinic acid, furfural, and hydroxymethylfurfural in water, Nonpolar. *Polar Aprotic and Protic Solvents Processes* 9:924. <https://doi.org/10.3390/pr9060924>
- Aida TM, Sato Y, Watanabe M, Tajima K, Nonaka T, Hattori H et al (2007) Dehydration of d-glucose in high temperature water at pressures up to 80 MPa. *J Supercrit Fluids* 40:381–388. <https://doi.org/10.1016/j.supflu.2006.07.027>
- Rasmussen H, Sørensen HR, Meyer AS (2014) Formation of degradation compounds from lignocellulosic biomass in the biorefinery: sugar reaction mechanisms. *Carbohydr Res* 385:45–57. <https://doi.org/10.1016/j.carres.2013.08.029>
- Patil SKR, Heltzel J, Lund CRF (2012) Comparison of structural features of humins formed catalytically from glucose, fructose,

- and 5-hydroxymethylfurfuraldehyde. *Energy Fuels* 26:5281–5293. <https://doi.org/10.1021/ef3007454>
29. Van Zandvoort I, Wang Y, Rasrendra CB, Van Eck ERH, Bruijninx PCA, Heeres HJ et al (2013) Formation, molecular structure, and morphology of humins in biomass conversion: influence of feedstock and processing conditions. *Chemsuschem* 6:1745–1758. <https://doi.org/10.1002/cssc.201300332>
 30. Maruani V, Narayanan-Richenapin S, Framery E, Andrioletti B (2018) Acidic hydrothermal dehydration of d -glucose into humins: identification and characterization of intermediates. *ACS Sustain Chem Eng* 6:13487–13493. <https://doi.org/10.1021/acssuschemeng.8b03479>
 31. Rasrendra CB, Windt M, Wang Y, Adisasmito S, Makertihartha IGBN, Van Eck ERH et al (2013) Experimental studies on the pyrolysis of humins from the acid-catalysed dehydration of C6-sugars. *J Anal Appl Pyrolysis* 104:299–307. <https://doi.org/10.1016/j.jaap.2013.07.003>
 32. Hong C, Wang Z, Si Y, Li Z, Xing Y, Hu J, et al (2021) Effects of aqueous phase circulation and catalysts on hydrothermal liquefaction (HTL) of penicillin residue (PR): characteristics of the aqueous phase, solid residue and bio oil. *Sci Total Environ* 776. <https://doi.org/10.1016/j.scitotenv.2021.145596>
 33. Luijkx GCA, Rantwijk, Bekkum V (1991) Formation of 1,2,4-benzenetriol by hydrothermal treatment of carbohydrates. Form 1,2,4-Benzenetriol by Hydrothermal Treat Carbohydrates 1:795–6. <https://doi.org/10.1136/bmj.1.5699.795>
 34. Abdelmoez W, Yoshida H, Nakahasi T (2010) Pathways of amino acid transformation and decomposition in saturated subcritical water conditions. *Int J Chem React Eng* 8. <https://doi.org/10.2202/1542-6580.1903>
 35. Cox JS, Seward TM (2007) The reaction kinetics of alanine and glycine under hydrothermal conditions. *Geochim Cosmochim Acta* 71:2264–2284. <https://doi.org/10.1016/j.gca.2007.01.020>
 36. Qiu Y, Aierzhati A, Cheng J, Guo H, Yang W, Zhang Y (2019) Biocrude oil production through the Maillard reaction between leucine and glucose during hydrothermal liquefaction. *Energy Fuels* 33:8758–8765. <https://doi.org/10.1021/acs.energyfuels.9b01875>
 37. Klingler D, Berg J, Vogel H (2007) Hydrothermal reactions of alanine and glycine in sub- and supercritical water. *J Supercrit Fluids* 43:112–119. <https://doi.org/10.1016/j.supflu.2007.04.008>
 38. Madsen RB, Biller P, Jensen MM, Becker J, Iversen BB, Glasius M (2016) Predicting the chemical composition of aqueous phase from hydrothermal liquefaction of model compounds and biomasses. *Energy Fuels* 30:10470–10483. <https://doi.org/10.1021/acs.energyfuels.6b02007>
 39. Rogalinski T, Liu K, Albrecht T, Brunner G (2008) Hydrolysis kinetics of biopolymers in subcritical water. *J Supercrit Fluids* 46:335–341. <https://doi.org/10.1016/j.supflu.2007.09.037>
 40. Fang X, Schmidt-Rohr K (2009) Fate of the amino acid in glucose-glycine melanoidins investigated by solid-state nuclear magnetic resonance (NMR). *J Agric Food Chem* 57:10701–10711. <https://doi.org/10.1021/jf9020587>
 41. Yaylayan VA (2003) Recent advances in the chemistry of strecker degradation and amadori rearrangement: implications to aroma and color formation. *Nippon Shokuhin Kagaku Kogaku Kaishi* 50:372–377. <https://doi.org/10.3136/nskkk.50.372>
 42. Wang Z (2011) Reaction mechanisms of hydrothermal liquefaction of model compounds and biowaste feedstocks. Order No. 3496768. University of Illinois at Urbana-Champaign. <https://www.proquest.com/dissertations-theses/reaction-mechanisms-hydrothermal-liquefaction/docview/921613432/se-2>
 43. Inoue S, Noguchi M, Hanaoka T, Minowa T (2004) Organic compounds formed by thermochemical degradation of glucose-glycine melanoidins using hot compressed water. *J Chem Eng Japan* 37:915–919. <https://doi.org/10.1252/jcej.37.915>
 44. Yaylayan VA, Kaminsky E (1998) Isolation and structural analysis of Maillard polymers: caramel and melanoidin formation in glycine/glucose model system. *Food Chem* 63:25–31. [https://doi.org/10.1016/S0308-8146\(97\)00237-9](https://doi.org/10.1016/S0308-8146(97)00237-9)
 45. Torri C, Garcia Alba L, Samori C, Fabbri D, Brilman DWF (2012) Hydrothermal treatment (HTT) of microalgae: detailed molecular characterization of HTT oil in view of HTT mechanism elucidation. *Energy Fuels* 26:658–671. <https://doi.org/10.1021/ef201417e>
 46. Subramanya SM, Savage PE (2021) Identifying and modeling interactions between biomass components during hydrothermal liquefaction in sub-, near-, and supercritical water. *ACS Sustainable Chem Eng* 9:13874–13882. <https://doi.org/10.1021/acssuschemeng.1c04810>
 47. Wang HY, Qian H, Yao WR (2011) Melanoidins produced by the Maillard reaction: structure and biological activity. *Food Chem* 128:573–584. <https://doi.org/10.1016/j.foodchem.2011.03.075>
 48. Adams A, Tehrani KA, Keršien M, Venskutonis R, De Kimpe N (2003) Characterization of model melanoidins by the thermal degradation profile. *J Agric Food Chem* 51:4338–4343. <https://doi.org/10.1021/jf0340254>
 49. Chacon-Parra AD, Hall PA, Lewis DM, Glasius M, Van Eyk PJ (2022) Elucidating the Maillard reaction mechanism in the hydrothermal liquefaction of binary model compound mixtures and spirulina. *ACS Sustain Chem Eng* 10:10989–11003. <https://doi.org/10.1021/acssuschemeng.2c03111>
 50. Liu S, Zhu Y, Liao Y, Wang H, Liu Q, Ma L et al (2022) Advances in understanding the humins: formation, prevention and application. *Appl Energy Combust Sci* 10:100062. <https://doi.org/10.1016/j.jaecs.2022.100062>

Publisher's note Springer Nature remains neutral with regard to jurisdictional claims in published maps and institutional affiliations.